Research Article

Temitope Love Baiyegunhi*, Kuiwu Liu, Oswald Gwavava, Christopher Baiyegunhi, and Maropene Rapholo

Geochemistry of the mudrocks and sandstones from the Bredasdorp Basin, offshore South Africa: Implications for tectonic provenance and paleoweathering

https://doi.org/10.1515/geo-2020-0260
received June 01, 2020; accepted April 29, 2021

Abstract: An inorganic geochemical investigation of mudrocks and sandstone from the southern Bredasdorp Basin, off the south coast of South Africa was carried out to unravel the provenance, paleoweathering, and tectonic setting of the basin. Seventy-seven representative samples from exploration wells E-AH1, E-AJ1, E-BA1, E-BB1, and E-D3 underwent geochemical analysis involving major and trace elements. The major oxide compositions show that the sandstones could be classified as sub-arkose and sublithic arenite. The provenance discrimination diagrams based on major oxide geochemistry revealed that the sandstones are mainly of quartzose sedimentary provenance, while the mudrocks are of quartzose sedimentary and intermediate igneous provenances. The discrimination diagrams indicate that the Bredasdorp sediments were mostly derived from a cratonic interior or recycled orogen. The bivariate plots of TiO_2 versus Ni, TiO_2 against Zr, and La/Th versus Hf as well as the ternary diagrams of V–Ni–Th∗10 suggest that the mudrocks and sandstones were derived from felsic igneous rocks. The tectonic setting discrimination diagrams support passive-active continental margin setting of the provenance. Also, the closely similar compositions of the analysed samples and recent sedimentary rocks of the East African Rift System perhaps suggest a rifted basin tectonic setting for the Bredasdorp Basin. Chemical index of alteration (CIA) indices observed in the sandstones suggest that their source area underwent low to moderate degree of chemical weathering. However, the mudrocks have high CIA indices suggesting that the source area underwent more intense chemical weathering, possibly due to climatic and/or tectonic variations.

Keywords: geochemistry, provenance, weathering, tectonic setting, bredasdorp basin

1 Introduction

The geochemistry of clastic sedimentary rocks is a vital tool used in the study of provenance, paleoweathering conditions, and tectonic setting as well as to constrain the geodynamic development and composition of the upper continental crust (UCC) [1,2]. The mineralogical and chemical compositions of these rocks are the products of numerous variables that include provenance, weathering conditions, transport, diagenesis, climate, and tectonism [3]. In geochemical studies, some designated trace elements such as La, Y, Sc, Cr, Th, Zr, Hf, Nb, and major oxides especially TiO_2 are sensitive indicators of the source rocks, provenance, paleoweathering and paleoclimatic conditions, and tectonic setting [3,4]. This is due to their comparatively low mobility and insolubility during sedimentary processes [5–7]. Furthermore, the relative distribution of the immobile trace elements with varying concentrations in felsic and basic rocks has been employed to deduce the relative contribution of felsic and basic sources in shales from different tectonic

* **Corresponding author: Temitope Love Baiyegunhi,** Department of Geology, Faculty of Science and Agriculture, University of Fort Hare, Private Bag X1314, Alice 5700, Eastern Cape Province, South Africa, e-mail: 201814648@ufh.ac.za
Kuiwu Liu, Oswald Gwavava: Department of Geology, Faculty of Science and Agriculture, University of Fort Hare, Private Bag X1314, Alice 5700, Eastern Cape Province, South Africa
Christopher Baiyegunhi: Department of Geology and Mining, School of Physical and Mineral Sciences, University of Limpopo, Private Bag X1106, Sovenga 0727, Limpopo Province, South Africa, e-mail: lovedestiny324@yahoo.com
Maropene Rapholo: Department of Geology and Mining, School of Physical and Mineral Sciences, University of Limpopo, Private Bag X1106, Sovenga 0727, Limpopo Province, South Africa

environments [8]. For example, trace elements like La and Th are enriched in felsic rocks, while Sc, Cr, and Co are more concentrated in basic rocks. Also, the relative reduction of oxides like Na_2O and CaO, and enrichment of TiO_2 and SiO_2 give important clues for tectonic setting. Therefore, the distribution of these major oxides and trace elements in mudrocks and sandstones gives evidences or clues to the geological processes, provenance, and tectonic settings of their respective sources [6–11].

Sandstones have been widely investigated for tectonic provenance using the traditional classic petrographic methods. However, in some instances, sandstones with a significant amount of fine fraction may contain trace element ratios that could provide added information about the provenance. On the other hand, shales are the most abundant type of sediment in sedimentary basins worldwide and they are alleged to represent average crustal provenance composition much better than sandstones [12,13]. In geochemical provenance studies, fine-grained sedimentary rocks like shales are considered to be the most useful rocks due to their homogeneity before deposition, post-depositional impermeability, and higher abundance of trace elements [3,14–16]. Several researchers including Bhatia [17] and Roser and Korch [18] have highlighted that major element geochemistry of the clastic sedimentary rocks are very useful in discriminating between different tectonic settings. In fact, they proposed the use of bivariate diagram of K_2O/Na_2O versus SiO_2 and calc-alkaline oxide ($CaO–Na_2O–K_2O$) ternary diagram to decipher tectonic setting of unknown basins. These diagrams are still widely used to unravel the tectonic setting of ancient basins. However, McLennan et al. [19] reported that the trace elements like La, Y, Sc, Cr, Th, Zr, Hf, and Nb, especially when used in combination with TiO_2, are most appropriate for provenance and tectonic setting determination studies due to their fairly low mobility during sedimentary deposition. Major element analysis is also applicable in interpreting paleoweathering and tectonic setting [3,20,21]. Immobile elements like Al, Ti, and Zr are also helpful when estimating the nature of source rock [3,22]. The index of compositional variability (ICV), K_2O/Al_2O_3 ratio, chemical index of alteration (CIA), and $Al_2O_3–(CaO + Na_2O)–K_2O$ (A–CN–K) ternary plots are useful geochemical parameters for the study of provenance and maturity of the rocks [23,24].

There have been quite a number of recent studies that investigated the elemental composition of mudrocks and sandstones with the aim of evaluating their provenance [6,11,25–28]. However, most of these studies widely used the traditional petrographic techniques in the calculation and interpretation of detrital modes of sandstones, and consequently, in the determination of their provenance and paleoweathering conditions [29,30]. In addition, the mineralogy of mudrocks, especially shale has been less considered or ignored due to the alteration of clay minerals during weathering and diagenesis [31]. Consequently, up to date, little attention has been paid to the study of provenance, paleoweathering, and tectonic setting of the Bredasdorp Basin, despite the hydrocarbon potential of the basin. Also, there is no known documented or reported classification of the Bredasdorp sandstones, and previous geochemical studies have successfully used geochemistry to solve problems associated with sandstone petrology. Geochemical classification of sandstones is worth attempting due to the fact that modern analytical methods are generating extensive datasets on the composition of rocks. Hence, this study was aimed at evaluating the geochemistry of the Bredasdorp mudrocks and sandstones in order to provide information on the chemical classification, source rock characteristics, provenance, paleoweathering, and tectonic setting using their major and trace elements geochemistry.

2 Geological setting

The Bredasdorp Basin is the westernmost sub-basin of the greater Outeniqua Basin (Figure 1). The basin was developed along the South African continental margin, underneath the Indian Ocean due to extensional episodes during the initial stage of rifting in the Late Jurassic–Early Cretaceous [32]. Sediments deposition in the Bredasdorp Basin was primarily controlled by the early continental rifting and tectonic development [32]. The basin serves as a depocentre and was predominantly infilled with Late Jurassic and Early Cretaceous marine and continental sediments [33]. The deposition of these syn-rift marine and continental sediment continued in the rift system until about 126 Ma, when most of the faulting stopped [34]. So, the syn-rift deposition commenced and subsequently initiated a transitional phase and thereafter a drifting phase [35]. The development of the Bredasdorp Basin is linked to the breakup of Gondwanaland and subsequent formation is associated with thermal subsidence in response to a single rifting event [36]. The tectonic development of the Bredasdorp Basin is summarised in Table 1.

The Bredasdorp Basin is envisaged to host an Oxfordian (~160 Ma) – recent stratigraphic column that overlies the rocks of the Cape Supergroup [35]. The Late Jurassic–Early Cretaceous shallow marine and fluvial syn-rift deposits underlie Albian to recent marine sediments [37]. The stratigraphic column shows the existence of a Middle Jurassic–Early Cretaceous syn-rift phase and it is

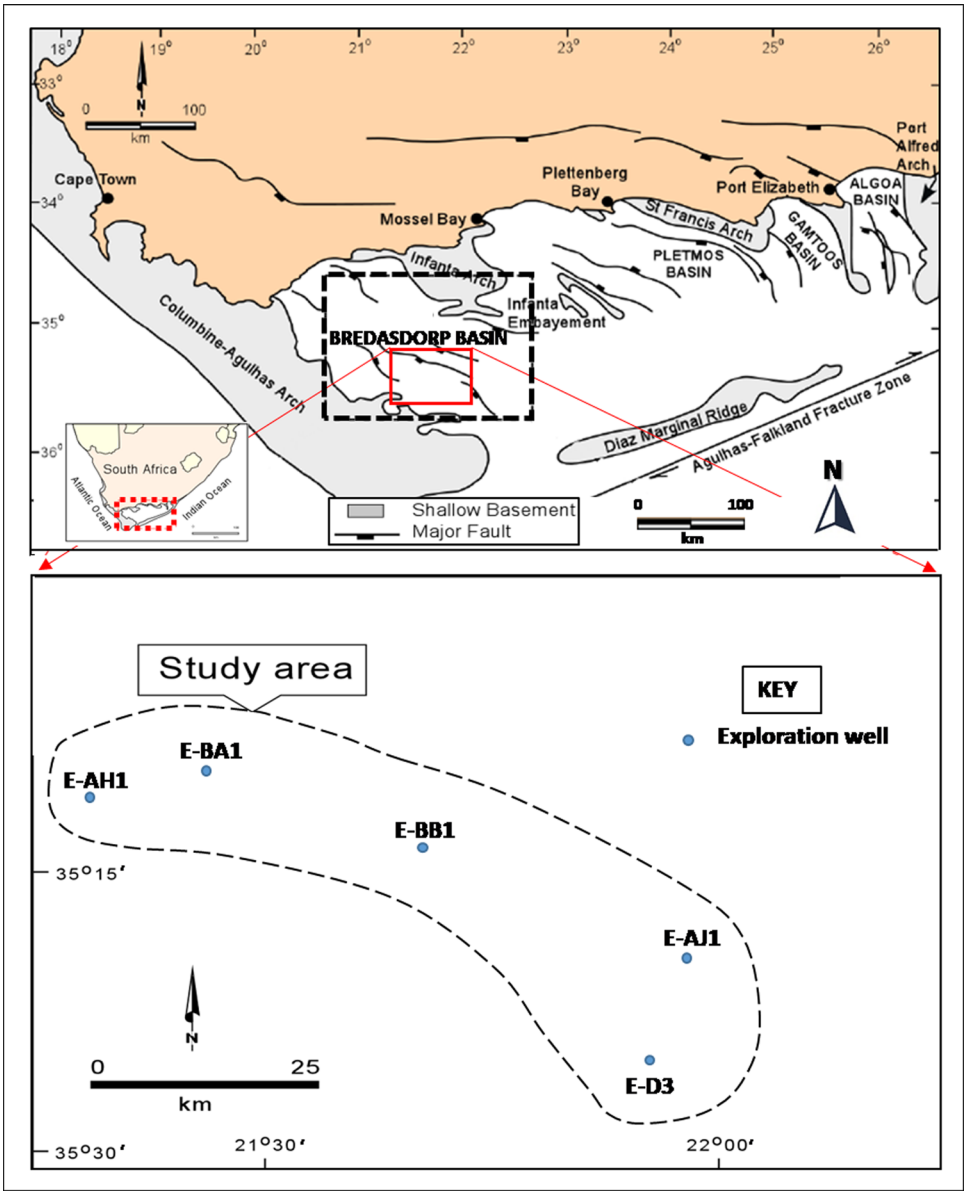

Figure 1: Map of the study area showing distribution of the exploration wells across the Bredasdorp Basin (modified from ref. [32]).

subsequently overlain by the early Cretaceous to Tertiary post-rift phase [37]. The syn-rift and drift (post-rift) sequences are separated by a regionally developed unconformity referred to as the 1At1, and it took place in the Lower Valanginian time [38] (Figure 2). The syn-rift sedimentation phases of the Bredasdorp Basin are subdivided into the syn-rift I and syn-rift II phases [39]. According to ref. [37], the syn-rift I phase occurred in the middle Jurassic–late Valanginian (Basement up to 1At1), whereas the syn-rift II took place in the Late Valanginian–Hauterivian (1At1–6At1).

In the northern part of the basin, the basal syn-rift deposits that occurred during the Kimmeridgian–late Valanginian are divided into four intervals (from base to top), namely the Lower Fluvial (LF), Lower Shallow Marine (LSM), Upper Fluvial (UF), and Upper Shallow Marine (USM) intervals. The above-mentioned intervals underlie the late Valanginian 1At1 regional unconformity [40] (Figure 2). The LF interval consists of mudrocks, sandstones, and conglomerates signifying an early graben fill deposition in an alluvial fan and fluvial environments [40]. On the other hand, the LSM interval points to the first marine invasion in the basin and it is made up of glauconitic sandstones, perhaps suggesting progradational anoxic marine deposits of the Kimmeridgian age [37,40]. The UF interval is made up of meandering fluvial and alluvial floodplain deposits, whereas the overlying USM interval is marked by the occurrence of massive glauconitic and fossil-rich sandstones of the Late Valanginian

Table 1: Summary of the structural development of the Bredasdorp Basin [42]

Stage	Period	Phase	Major event
1	Middle Jurassic–Valanginian (Basement–1At1)	Syn-rift I	Extension-instigated or driven subsidence and syn-rift basin fill. Isostatic uplift on both sides of the half-graben led to significant reduction in the erosion of syn-rift I sediments. Great or intensive marginal uplift and erosion of the northern part of the basin removed the whole syn-rift I succession in some places
2	Late Valanginian–Hauterivian (1At1–6At1)	Syn-rift II	Fast subsidence and extensive flooding. Continued or non-stop uplift caused additional truncation or reduction in structural highs. The deposition of deep water sediments happened within rift depocentres (southern sub-Basin and Arniston half-graben) led to the deposition of source rocks
3	Hauterivian–Aptian (6At1–13At1)	Transitional (Early drift)	Progradation enlargement of the shelf in the northern part over the Arniston half-graben, plus a sustained deepening of the southern sub-basin
4	Aptian–Maastrichtian (13At1–15At1)	Middle drift	Regional subsidence instigated by thermal cooling and sediment loading. Continued movement on the Arniston Fault
5	Paleocene–present day (15At1–seafloor)	Late drift	Oil-prone source in syn-rift depocentres and northern and central part of the Bredasdorp Basin proceed into the main phase of oil generation. Continued slight subsidence interrupted by the early tertiary alkaline intrusion activity over the central part of the basin. Late slanting of the basin together with uplift of the northern side led to the late removal or erosion of about 600 m succession in some places

age. Broad et al. [40] reported that these massive glauconitic fossiliferous sandstones were laid down as transgressive beach facies along the northern and southern edges of the Bredasdorp Basin and it extends into the neighbouring sub-basins.

The syn-rift I succession is terminated by the 1At1 regional unconformity, separating deep-marine sediments from the underlying USM sediments. This 1At1 unconformity signifies the beginning of a renewed rifting (syn-rift II) phase initiated due to early or initial movement along the Agulhas–Falkland Fracture Zone at approximately 133 Ma (Valanginian–Hauterivian boundary) [39]. The syn-rift II was later followed by the Transitional (early drift) phase, which occurred during Hauterivian–Early Aptian (6At1–13At1) [37] (Figure 2). The Transitional (early drift) phase was dominated by recurrent episodes of progradation and aggradation and it was mostly affected by tectonic events and eustatic sea-level changes [36,40]. The Transitional phase is considered the first deep water deposits in the Bredasdorp Basin and they were deposited due to major subsidence of the basin as well as an increase in water depth. On the other hand, the late drift phase trailed a major marine regression in the Bredasdorp Basin during the early Aptian [39]. This regression event resulted in a major erosion which is marked by the 13At1 unconformity. The erosion period is followed by a marine transgression, which carried and deposited organic-rich mudstone, shale, or claystone in the basin under an anoxic condition [35]. The onset of the late drift phase is manifested or noted by the 14At1 mid Albian unconformity (Figure 2), which marks the beginning of the active thermally instigated subsidence when the Columbine-Agulhas Arch was cleared by the trailing edge of the Falkland Plateau in the late Albian [40–42].

3 Methodology

A total of seventy-seven representative mudrock and sandstones collected from exploration wells E-AH1, E-AJ1, E-BA1, E-BB1, and E-D3 (Figure 1) were studied under the petrographic microscope and analysed for the major oxides and trace element concentrations. X-ray fluorescence (XRF) analysis was performed at the geochemical laboratory in the Department of Geology and Mining, University of Limpopo, South Africa. The rock samples were neatly cleaned and crushed into smaller sizes using the Braun Chipmunk VD67 jaw crusher. Thereafter, the Herzog milling machine was used to mill the crushed samples into powdery form of grain size less than 50 μm. Pressed pellets were used for the major oxides and trace elements analyses. The pressed pellets were analysed by

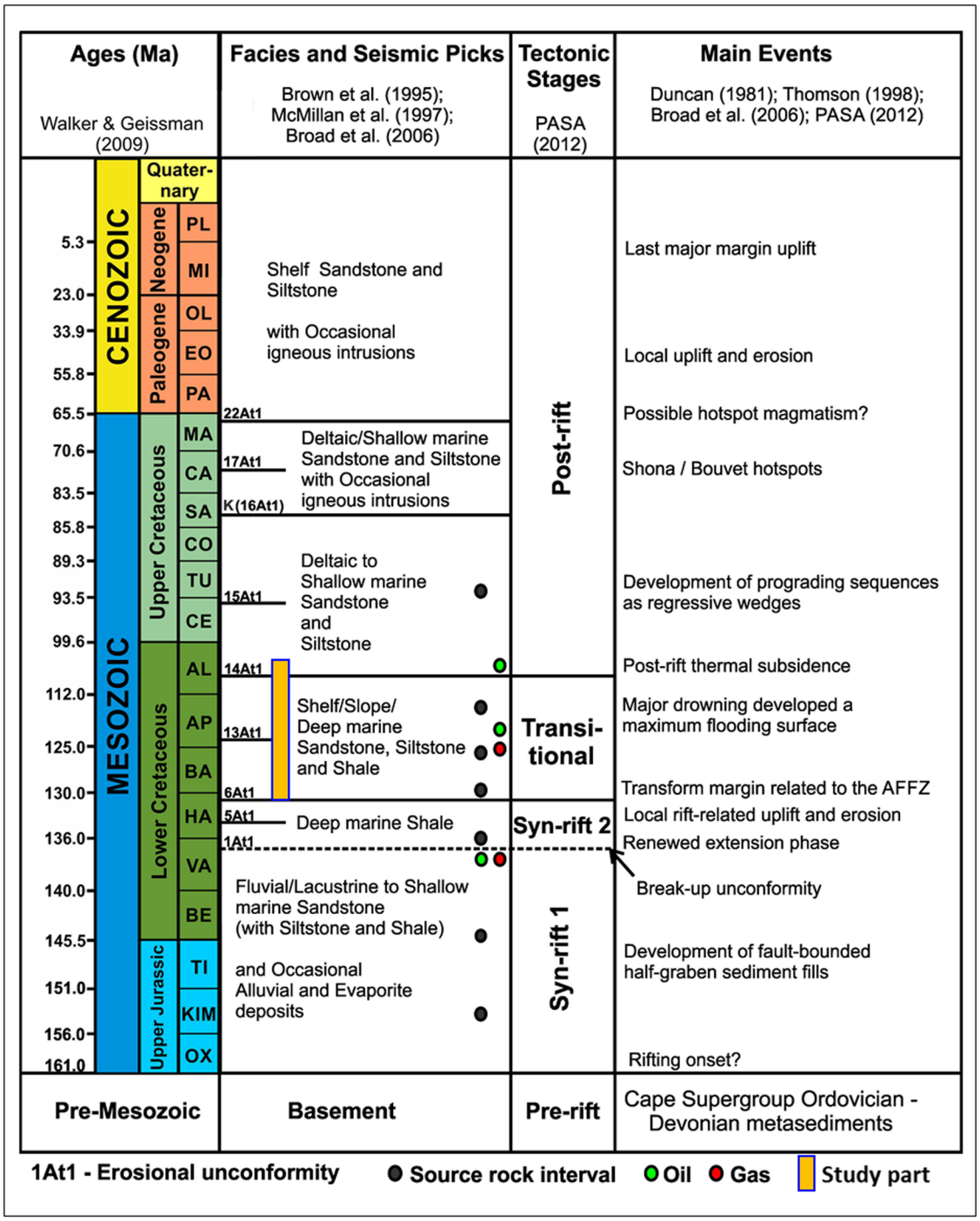

Figure 2: Stratigraphic chart of the Bredasdorp Basin showing the main unconformities and tectonic stages with corresponding geodynamic events (after ref. [34]).

PANalytical Zetium XRF spectrometer equipped with a 4 kW Rh tube. The milled samples were also dried at 100°C (Weight A) and heated at 1,000°C (Weight B) for a period of at least 3 h to oxidize S and Fe^{2+} in order to determine the loss of ignition (LOI). The mathematical expression for the percentage LOI is given as:

$$\%\ \mathrm{LOI} = \frac{\mathrm{Weight_A} - \mathrm{Weight_B}}{\mathrm{Weight_A} - \mathrm{Weight_{crucible}}} \times 100.$$

The Epsilon software program was used to quantify the oxides and trace elements in the mudrocks and sandstones. Discriminatory binary and ternary plots of the major oxides and trace elements were used for geochemical

classification as well as the determination of provenance and tectonic settings. In addition, CIA, chemical index of weathering (CIW), plagioclase index of alteration (PIA), and ICV were calculated and bivariate diagram of ICV against CIA and ternary diagram of Al_2O_3–(CaO + Na_2O)–K_2O were plotted to deduce the degree of weathering. In the CIA, CIW, PIA, and ICV formulas, CaO^* is the amount of CaO added into the silicate fraction of the rocks. In this study, rectification for CaO from the carbonate contribution was not carried out because of the absence of CO_2 value. Hence, the proposed method from ref. [43] was used to calculate the amount of CaO^* from the silicate fraction. The method suggested that CaO values should be accepted only if CaO < Na_2O. However, when CaO > Na_2O, it was alleged that the concentration of CaO is the same as that of Na_2O. This procedure measures the ratio of the secondary aluminous mineral to feldspar, and forms a basis for measuring the intensity of weathering.

4 Results

4.1 Petrography

The Bredasdorp sandstones are mostly composed of quartz, feldspar, glauconite, and clay minerals. The quartz, feldspar, and glauconite are the framework minerals, while the clay minerals are mostly the matrix and sometimes act as cement. The observed cements in the sandstones are authigenic clay mineral cement, quartz cement, and occasional glauconite cements. Texturally, these sandstones are moderately sorted to moderately well-sorted and of fine to medium grain sizes (Figures 3 and 4). Petrographic observations revealed that borehole E-AH1 consists mostly of massive, well-sorted, fine- to medium-grained glauconitic sandstone and claystone with minor siltstone interbeds. The claystones are characterised by near-horizontal bedding and sediment injection features (sandstone into claystone) near the contacts with the sandstones. Borehole E-AJ1 is made up of claystones and siltstones with occasional interbedded sandstones. The sandstones in borehole E-AJ1 are generally massive (structureless), fine to medium grained, and contain abundant glauconite and are moderately well-sorted. A distinctive feature in borehole E-AJ1 is the occurrence of stylolites, which are seen as irregular, undulatory, and coarsely sutured horizontal features and less commonly as finely sutured regular vertical to sub-vertical fractures. Borehole E-BA1 comprises mostly of massive moderately well-sorted, fine- to medium-grained glauconitic sandstone with minor claystone and siltstone. The sandstone is slightly porous, light brownish-grey with very fine to medium, well-sorted subangular grains. In addition, it is non-calcareous, slightly glauconitic, and slightly pyritic and contains green lithic fragments. The sandstone in borehole E-BB1 is mostly well-sorted, fine grained, very lithic (metaquartzite clasts), glauconitic, and slightly shelly and carbonaceous. In borehole E-D3, the sandstones are massive, moderately sorted, medium grained, and slightly glauconitic. In general, the roundness of the grains in the studied sandstone samples vary from subangular to rounded and the sphericity ranges from low to high (mostly low; oblong grains). The grain packing is irregular, showing both fairly packed and tightly packed grains. However, in most cases, the grains are moderately tight. Furthermore, the grain contact patterns vary from point contact to sutured contact, but predominantly long and concavo-convex contacts. The sandstone grains are often cemented or supported by clay matrix; however, some are grain supported. The change in grain size in the vertical succession indicates both regressive and transgressive conditions, although the transgressive conditions tend to dominate. The stratigraphy of the studied boreholes is presented in the supplementary data (Figure A1).

4.2 Major oxides

The major oxide concentrations in the Bredasdorp mudrocks and sandstones are presented in supplementary data (Table S1). The stratigraphic descriptions of the boreholes are presented in the supplementary data. The major oxide compositions are relatively variable, but are still comparable with the average compositions of oxides reported in refs [44–46] (supplementary data; Table S2). The studied samples have high percentages of SiO_2, varying between 51.70 and 81.58%. The concentration of Al_2O_3, CaO, Fe_2O_3, MgO, and K_2O ranges from 2.82 to 29.01%, 0.80 to 7.68%, 0.27 to 5.75%, 0.39 to 5.68%, and 0.43 to 5.11%, respectively. The percentages of MnO, TiO_2, Na_2O, and P_2O_5 are generally low, ranging from 0.01 to 0.10%, 0.16 to 0.99%, 0.03 to 1.30%, and 0.11 to 1.37%, respectively. The SiO_2 content in sandstones are higher than shales. In contrast, the concentration of Fe_2O_3, K_2O, and TiO_2 are higher in the mudrocks, depicting their association with clay-sized phases.

To compare the abundances of the oxides, the concentration of the major oxides in the studied samples were plotted against the concentration of Al_2O_3, as shown in Figures 5 and 6. The Al_2O_3 contents were used as a

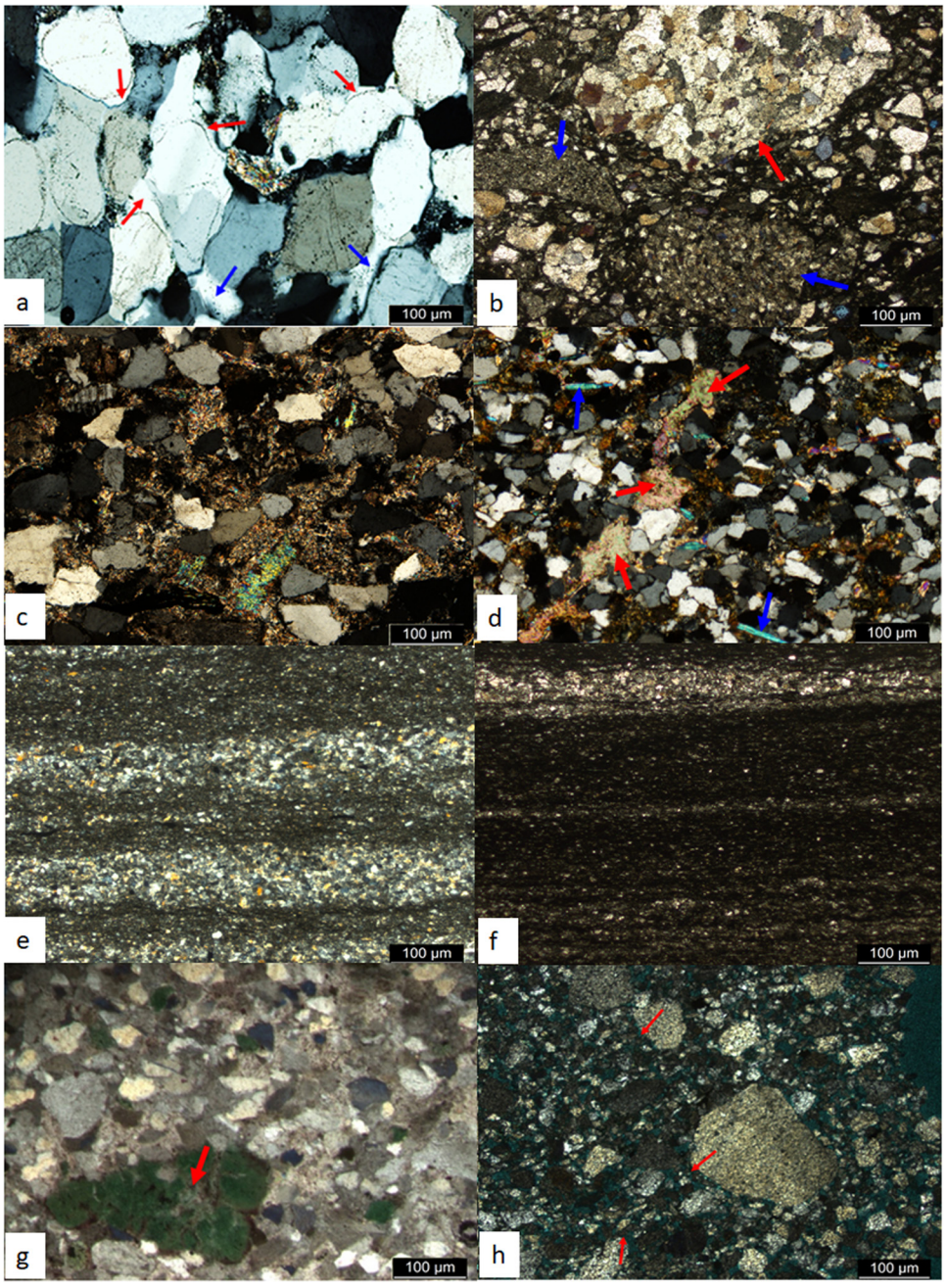

Figure 3: Thin section photomicrographs showing: (a) authigenic quartz (blue arrows) and quartz overgrowths (red arrows) in sandstone from borehole E-D3; (b) sedimentary lithic fragment (red arrow) and metamorphic lithic fragment (blue arrows) in sandstone from borehole; (c) mica in clay matrix in sandstone from borehole E-BA1; (d) calcite cement and mica flakes (blue arrows) in sandstone from borehole E-BB1; (e and f) claystone and siltstone layers in mudrock from borehole E-AH1; (g) partial replacement of feldspar and matrix by glauconite (red arrows) in sandstone from borehole E-AJ1; and (h) authigenic glauconite as rim or line on the grain surfaces (red arrows) in sandstone from Borehole E-AJ1.

normalisation factor because of its immobile nature during weathering, diagenesis, and metamorphism [47]. Furthermore, the average percentages of the Post-Archaean Australian Shale (PAAS) and UCC were taken from refs [3,48], respectively, and incorporated in the plots for comparison purposes. In the mudstone and shale samples, the concentration of SiO_2, Fe_2O_3, MgO, and Na_2O shows negative correlation with Al_2O_3, while the concentrations of TiO_2, MnO, CaO, K_2O, and P_2O_5 show no specific trend (Figure 5). On the other hand, all the major oxides in the sandstones

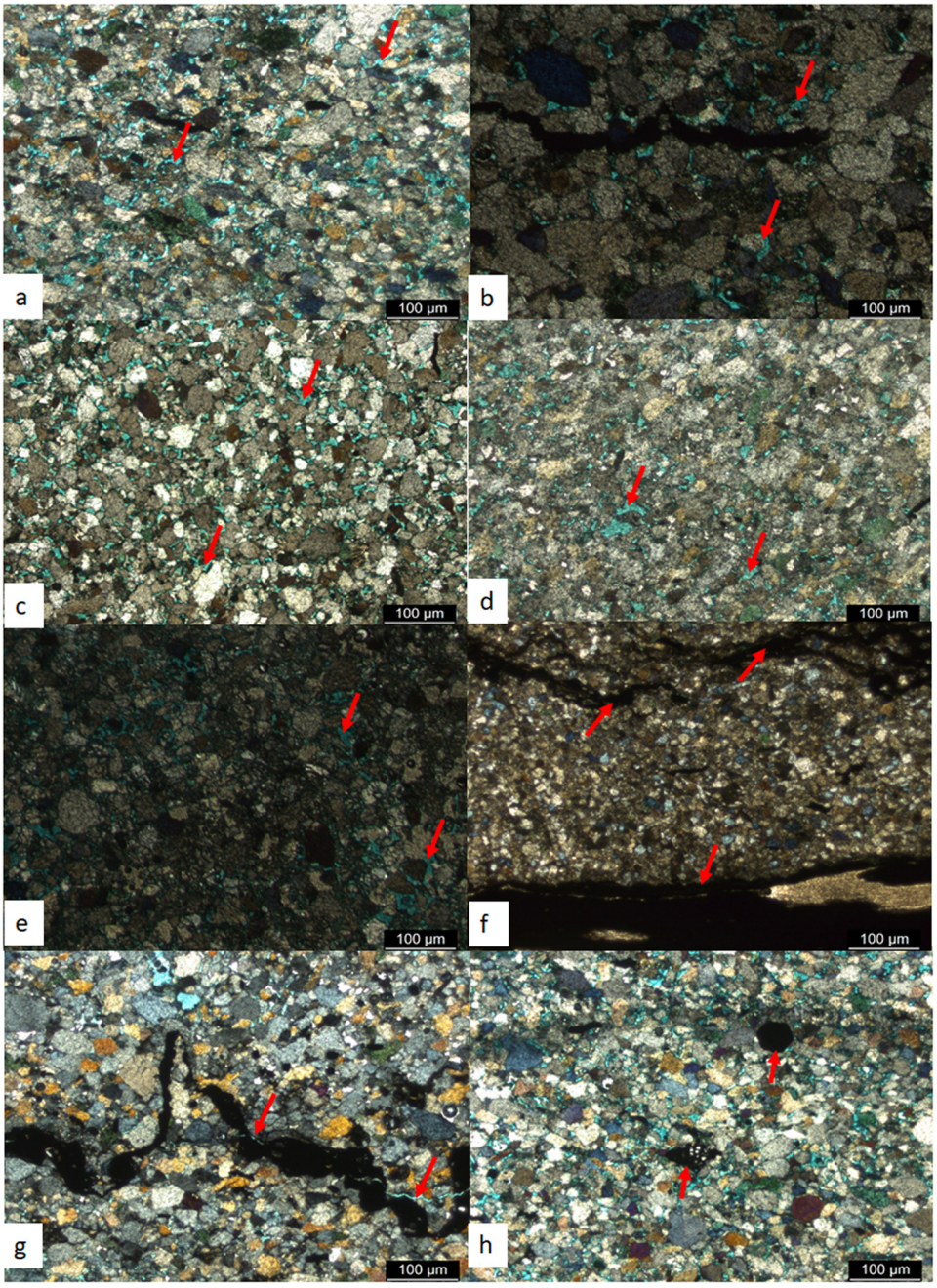

Figure 4: Thin section photomicrographs of sandstone showing (a–e) Primary porosity in Boreholes E-AH1, E-AJ1, E-BA1, E-BB1, and E-D3, respectively; (f and g) fractured pores (red arrows) in-filled by solid bitumens in Borehole E-BB1; and (h) oil emplacement in Borehole E-AJ1.

show no particular trend or correlation with Al_2O_3 (Figure 6). The positive correlations of some of the oxides in the mudstones and shales suggest their association with micaceous/clay minerals. The concentration of oxides in the mudrocks and sandstones were also normalised with those of UCC and PAAS (Figure 7). Relative to UCC, the average concentrations of SiO_2, TiO_2, Al_2O_3, Fe_2O_3, MnO, MgO, CaO, Na_2O, K_2O, and P_2O_5 in the mudrocks are 0.85, 1.05, 1.61, 0.83, 0.49, 0.65, 0.47, 0.24, 1.16, and 1.13, respectively. Relative to PAAS, the average concentrations of SiO_2, TiO_2, Al_2O_3, Fe_2O_3, MnO, MgO, CaO, Na_2O, K_2O and P_2O_5 in the mudrocks are 0.91, 0.68, 1.32, 0.58, 0.44, 0.74, 1.30, 0.67, 0.88, and 1.00, respectively.

Relative to UCC, the mudrocks are low in MnO, CaO, Na_2O, and very high in Al_2O_3. As reported in ref. [49], aluminium (Al) is simply absorbed on clays and concentrated in the finer, more weathered materials. In support of this, XRD analysis of the mudrocks revealed that they

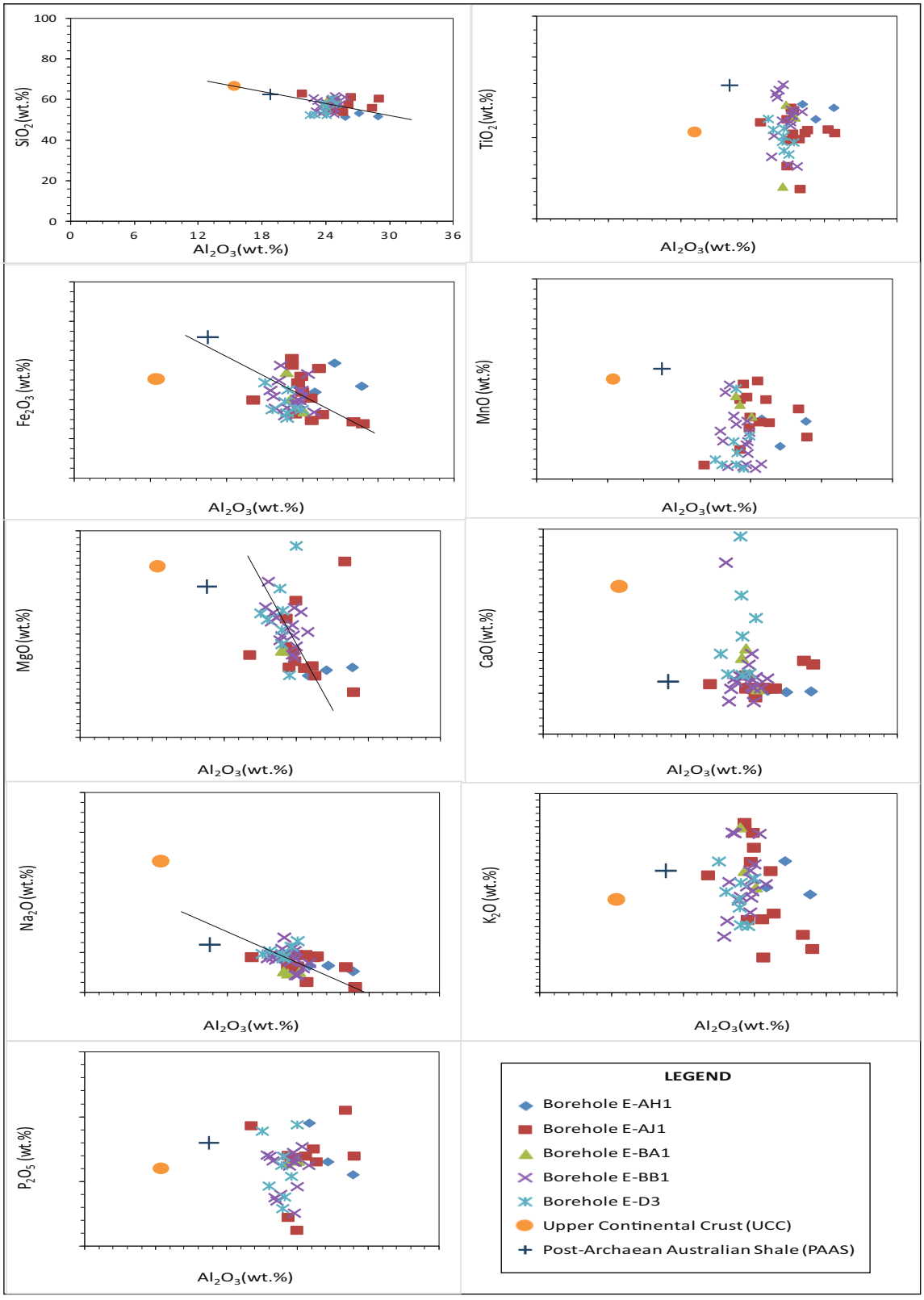

Figure 5: Major elements versus Al_2O_3 graph showing the distribution of shale samples from the Bredasdorp Basin. Average PAAS and UCC values were extracted from refs [3,48], respectively, and plotted for comparison.

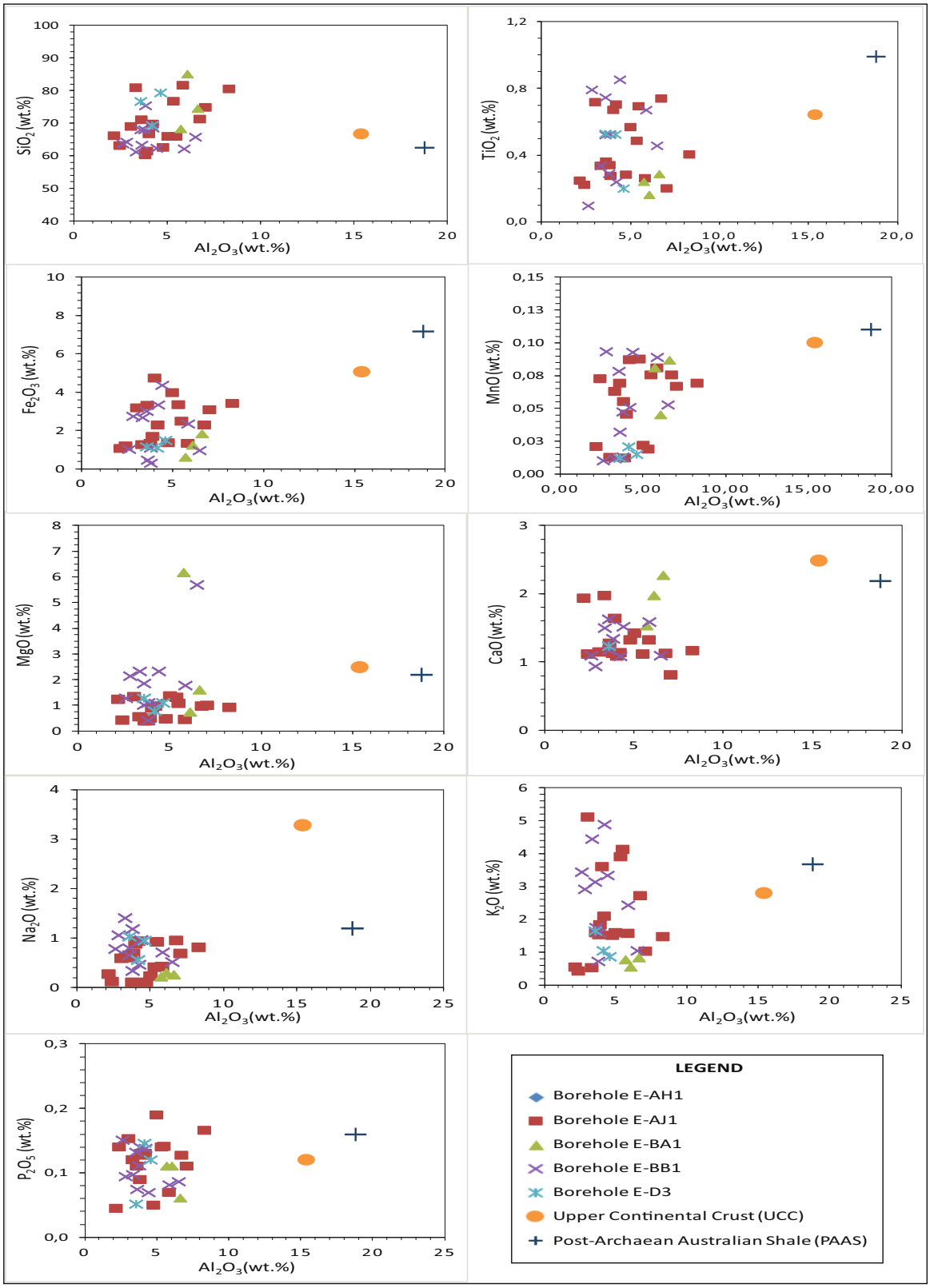

Figure 6: Major elements versus Al_2O_3 graph showing the distribution of sandstone samples from the Bredasdorp Basin. Average PAAS and UCC values were extracted from refs [3,48], respectively, and plotted for comparison.

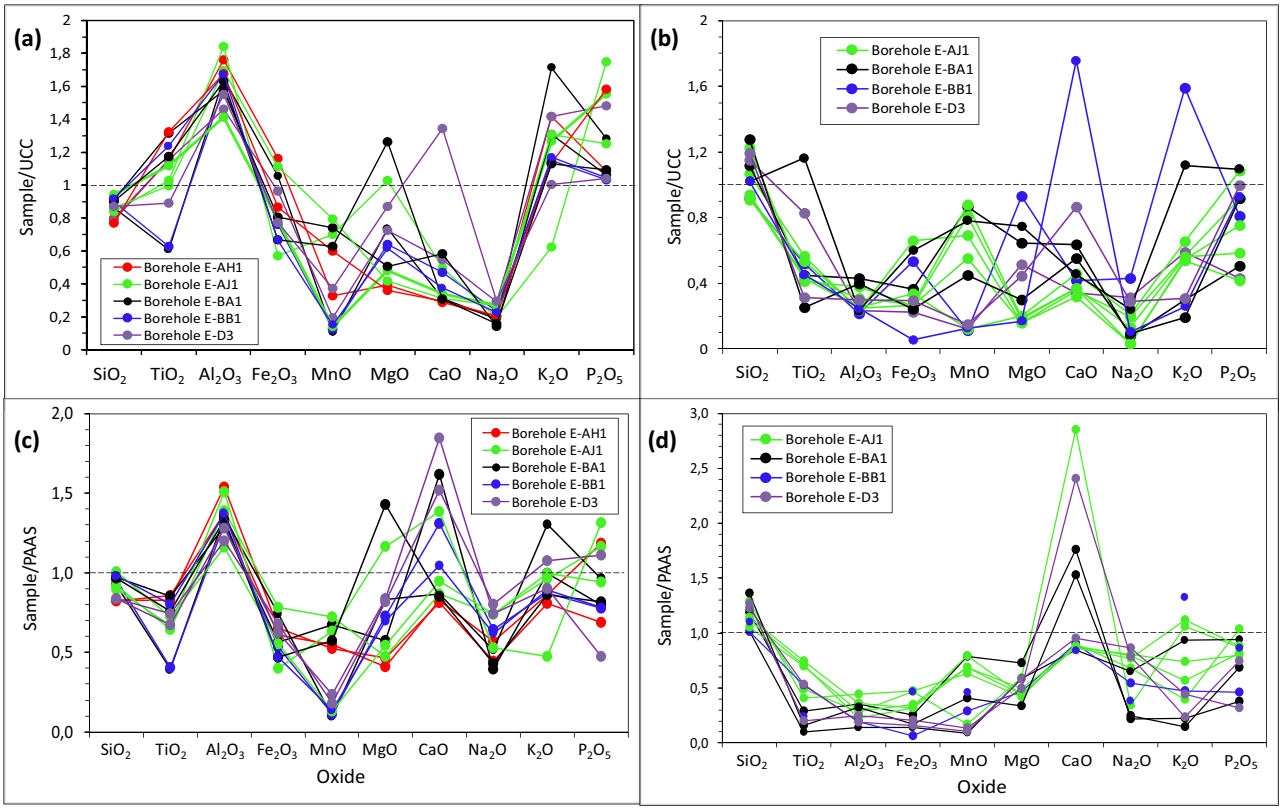

Figure 7: (a) Spider plot of oxides for the Bredasdorp mudrocks normalised against UCC (after ref. [48]); (b) Spider plot of oxides for the Bredasdorp sandstones normalised against UCC (after ref. [48]); (c) Spider plot of oxides for the Bredasdorp mudrocks normalised against PAAS (after ref. [3]); and (d) Spider plot of oxides for the Bredasdorp sandstones normalised against PAAS (after ref. [3]).

are dominated with the mineral kaolinite ($Al_2Si_2O_5(OH)_4$). The concentration of these oxides in the mudrocks are generally comparable with those of PAAS. On the other hand, relative to UCC, the average concentrations of SiO_2, TiO_2, Al_2O_3, Fe_2O_3, MnO, MgO, CaO, Na_2O, K_2O, and P_2O_5 in the sandstones are 1.04, 0.69, 0.29, 0.41, 0.52, 0.56, 0.50, 0.19, 0.74, and 0.93, respectively. The average concentrations of Al_2O_3, Fe_2O_3, and Na_2O are low as compared to the UCC values. The depletion of Na_2O (<1%) in the Bredasdorp rocks can be linked to the relatively smaller amount of Na-rich plagioclase in them, which is consistent with the petrographic results. The concentration of K_2O and Na_2O, and their ratios (K_2O/Na_2O >1) are also consistent with the petrographic observations, which revealed that K-feldspar dominates over plagioclase (albite) feldspar. The enrichment of K_2O relates to the presence of illite as common clay mineral in the shales and sandstones. In addition, the enrichment of CaO can be attributed to the presence of diagenetic calcite cement, which is also consistent with the petrographic results. In comparison with PAAS, the average concentrations of SiO_2, TiO_2, Al_2O_3, Fe_2O_3, MnO, MgO, CaO, Na_2O, K_2O, and P_2O_5 in the sandstones are 1.11, 0.54, 0.24, 0.29, 0.51, 0.63, 1.40, 0.53, 0.56, and 0.70, respectively. Again, the average concentrations of Al_2O_3 and Fe_2O_3 are low as compared to PAAS.

4.3 Trace elements

The trace element concentrations in mudrocks and sandstones are presented in the supplementary data (Table S3a–b). The concentrations (in ppm) of these elements are fairly variable but still comparable with those average concentrations reported by refs [45,46,50,51] (supplementary data; Table S4). The concentration of large ion lithophile elements (LILE) like Rb, Ba, Sr, and Th in the studied samples are in range of 12.60–267.30, 55.20–1160.00, 29.80–324.70, and 4.50–16.50 ppm, respectively. The concentration of the high field strength elements (HFSE) such as Zr, Y, and Nb varies from 50.00 to 215.80 ppm, 1.00 to 127.70 ppm, and 2.70 to 40.80 ppm, respectively. Likewise, transition trace elements (TTE) like Sc, V, Cr, Ni, and Zn vary in the range of 1.80–4.90, 16.50–238.00, 247.70–592.80, 5.20–38.30, and 5.50–241.30 ppm, respectively. In general, sandstones have higher concentration of Ba, Th, Y, Nb, Sc, V, and Cr than the mudrocks, while the

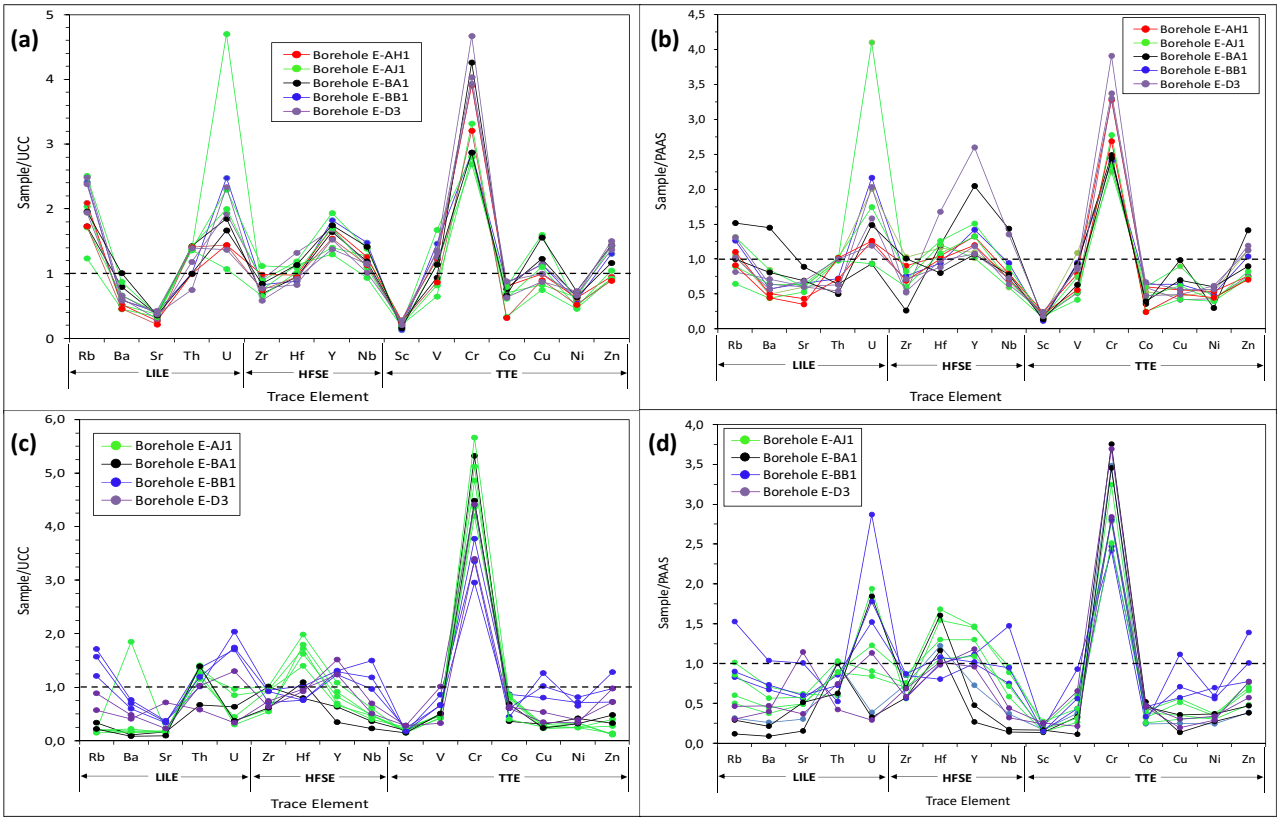

Figure 8: (a) UCC-normalised trace elements distribution of mudrocks from the Bredasdorp Basin. The UCC values are from ref. [48]; (b) PAAS-normalised trace elements distribution of mudrocks from the Bredasdorp Basin. The PAAS values are from ref. [3]; (c) UCC-normalised trace elements distribution of sandstones from the Bredasdorp Basin. The UCC values are from ref. [48]; and (d) PAAS-normalised trace elements distribution of sandstones from the Bredasdorp Basin. The PAAS values are from ref. [3].

content of Rb, Sr, Zr, Ni, and Zn are higher in the mudrocks than the sandstones.

4.3.1 LILE: Rb, Ba, Sr, Th, and U

The concentration of the LILE in the mudrocks are generally comparable to those of UCC and PAAS. However, the concentrations of U and Cr are high, whereas Sr content is relatively low (Figure 8a and b). On the other hand, the concentration of Th in the sandstones is relative to UCC and PAAS. Although U content is comparable to UCC, it is high relative to PAAS. In addition, the concentrations of Rb, Ba, and Sr in the sandstones are generally low when compared to the UCC and PAAS values (Figure 8c and d). Th and Nb are positively correlated in the mudrocks and sandstones, perhaps suggesting that it may have been controlled by clays and/or other phases (i.e. Ti- and Nb-bearing phases) associated with clay minerals. Also, Rb has positive correlations with Ba in the mudrocks and sandstones, possibly indicating the same geochemical characteristics. These correlations show that their distributions are mostly controlled by illites with little contribution from other clay minerals.

4.3.2 HFSE: Zr, Hf, Y, and Nb

HFSE elements are often concentrated in felsic rocks than mafic rocks [52]. The Zr, Hf, Nb, and Y contents in the mudrocks and sandstones are comparable to UCC and PAAS contents (Figure 8a and c), although Zr is relatively low, whereas Y is fairly high (Figure 8b and d).

4.3.3 TTE: Sc, V, Cr, Co, Cu, Ni, and Zn

The TTE in the Bredasdorp mudrocks and sandstones are depleted in comparison with the UCC and PAAS. In the mudrocks, V, Cu, and Zn are relatively comparable with UCC and PAAS, whereas the concentrations of Sc, Co, and Ni are low relative to UCC and PAAS (Figure 8).

Furthermore, the concentration of Cr in the samples are generally high when compared to the UCC and PAAS.

5 Interpretations and discussion

5.1 Sandstone classification

The concentrations of silica, aluminium, potassium, sodium, and iron oxides have been used to classify sandstones [53,54]. The background geochemical classification diagrams of refs [53,54] were used to classify the Bredasdorp sandstones. Based on the Herron's classification [54] scheme, the Bredasdorp sandstones are mainly sub-arkose and sub-lithic arenite (Figure 9). Similarly, the classification scheme in ref. [53] shows that the sandstones are sub-arkose and sub-lithic arenite, while the mudrocks are plotted in the field of shale (Figure 10). The geochemical classification of the sandstones is also in agreement or consistent with the petrographic classification of the sandstones.

5.2 Provenance

The major oxide concentrations in the mudrocks and sandstones have been used to decipher the provenance of the Bredasdorp rocks using the discriminant functions analysis proposed in ref. [55]. The bivariate plot of the discriminant functions discriminates between quartzose sedimentary or recycled, felsic igneous, intermediate igneous, and mafic igneous provenance fields. The mudrock samples are plotted in both the quartzose sedimentary provenance and felsic igneous provenance fields (Figure 11a), whereas the sandstones fall within the quartzose sedimentary provenance field (Figure 11b).

The bivariate plot of TiO_2 versus Zr shows that the mudrocks and sandstones are mostly from felsic igneous rocks with little contribution from intermediate igneous rocks (Figure 12). Also, the binary plot of TiO_2 against Ni, La/Th versus Hf, and V–Ni–Th∗10 ternary diagram revealed that the source area for most of the Bredasdorp mudrocks and sandstones are predominantly acidic or felsic in nature (Figures 13–15). The concentration of HFSE (i.e. Hf) are higher in the sandstones than the shale samples. The low content of Hf and elemental ratios like La/Sc and Th/Sc indicate the presence of fractionated source rocks with lower compatible element contents and recycled sediments in the source area. Also, the variation in chemical composition, perhaps suggests changes in the supply of material and a fluctuation in physico-chemical environment of deposition. The pattern of geochemical behaviour of individual element shows that most of the trace elements that found their way into the ancient sediments seem to have invaded the lattices of the silicates and clay minerals and structurally combined with them.

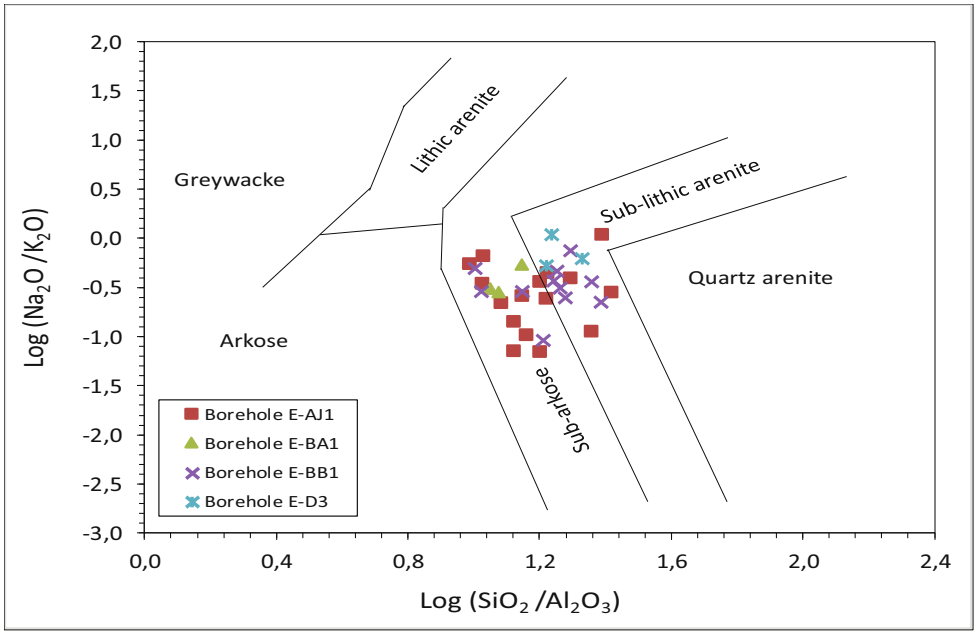

Figure 9: Geochemical classification of the Bredasdorp sandstones based on the binary of plot of Log (Na_2O/K_2O) versus Log (SiO_2/Al_2O_3) (after ref. [53]).

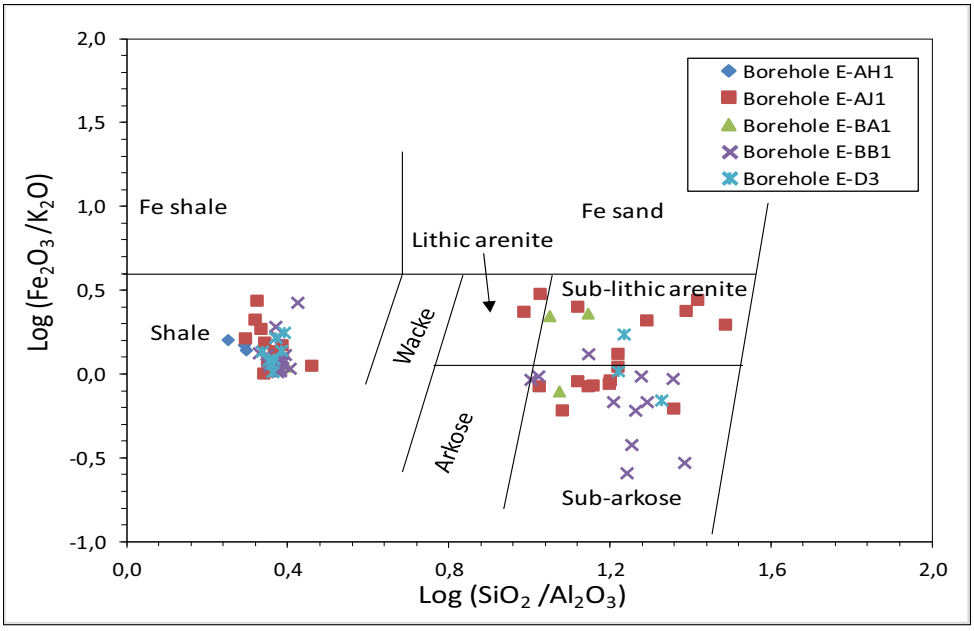

Figure 10: Geochemical classification of the Bredasdorp samples based on the binary of plot of Log (Fe_2O_3/K_2O) versus Log (SiO_2/Al_2O_3) (background field after ref. [54]).

5.3 Tectonic setting of the source area

The chemical compositions of clastic rocks are greatly influenced by plate tectonic settings of their source area(s) and depositional basins [4,17]. Consequently, clastic rocks often have distinctive geochemical signatures or characteristics for a particular tectonic setting. As reported in ref. [7], tectonic setting discrimination ternary diagrams offer a steadfast outcome for clastic rocks that have not been sturdily affected by post-depositional weathering and metamorphism. The binary plots of major oxides and trace elements' geochemistry have been widely used by several researchers to infer the tectonic setting of clastic rocks [4,17,18,58–60]. The major oxides and trace elements

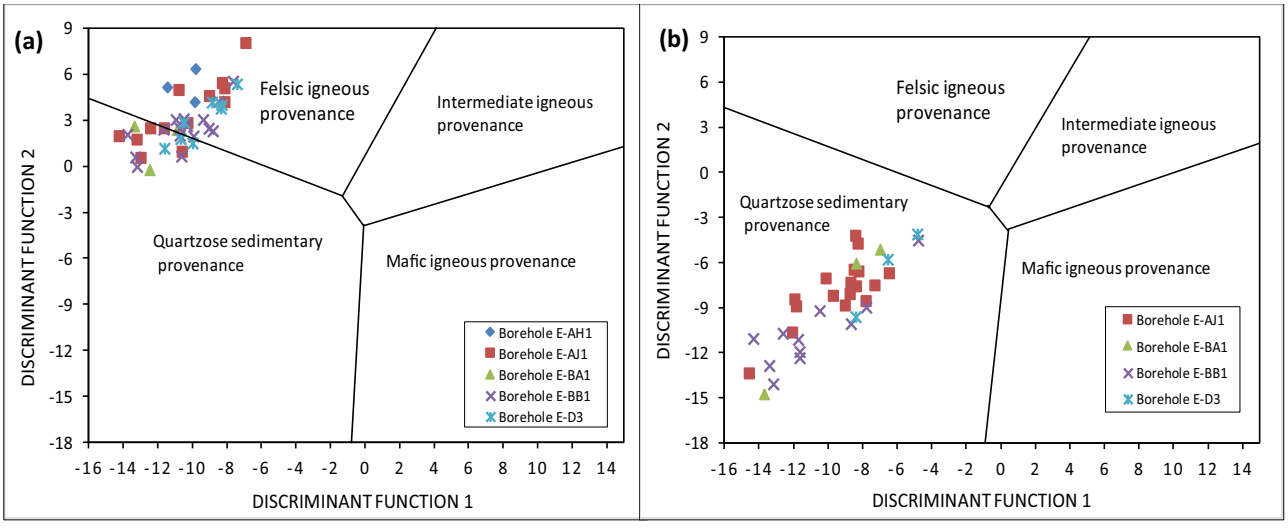

Figure 11: Major oxides discriminant function diagram showing provenance for the Bredasdorp Basin. (a) mudrocks; and (b) sandstones (background field after ref. [55]). The discriminant functions are: Discriminant Function 1 = (−1.773 TiO_2) + (0.607 Al_2O_3) + (0.760 Fe_2O_3) + (−1.500 MgO) + (0.616 CaO) + (0.509 Na_2O) + (−1.224 K_2O) + (−9.090); and Discriminant Function 2 = (0.445 TiO_2) + (0.070 Al_2O_3) + (−0.250 Fe_2O_3) + (−1.142 MgO) + (0.438 CaO) + (1.475 Na_2O) + (−1.426 K_2O) + (−6.861).

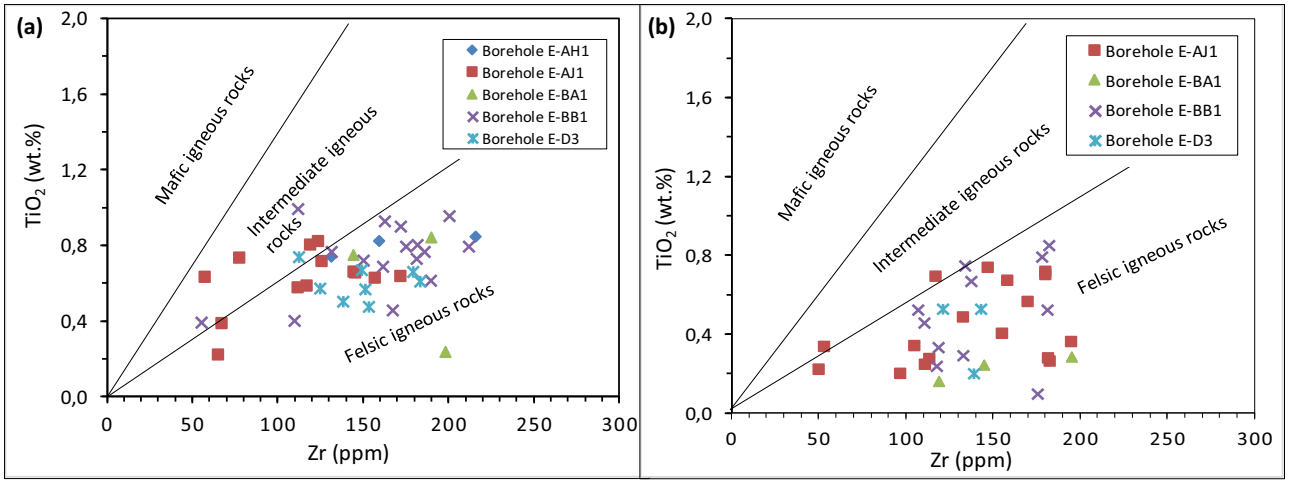

Figure 12: Bivariate plot TiO_2 against Zr showing provenance for the Bredasdorp Basin: (a) mudrocks and (b) sandstones (background field after ref. [20]).

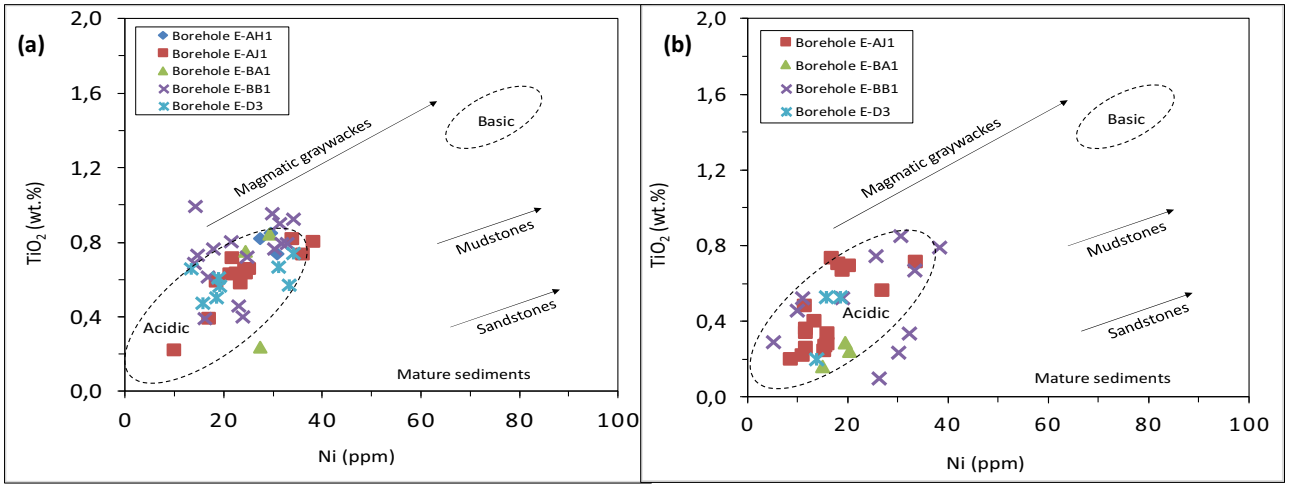

Figure 13: Binary plot of TiO_2 versus Ni showing acidic source area for the Bredasdorp Basin: (a) mudrocks and (b) sandstones (background field after ref. [56]).

tectonic discriminate diagrams of refs [4,18,59] have been attempted in this study to deduce the tectonic setting for the Bredasdorp mudrocks and sandstones. These aforementioned discrimination diagrams divide tectonic settings into oceanic island arc (OIA), continental island arc (CIA), active continental margin (ACM), and passive continental margin (PM).

The binary plot of Log (K_2O/Na_2O) against SiO_2 in the background tectonic setting discrimination diagram of ref. [18] shows that most of the Bredasdorp mudrocks are plotted in the ACM field, while a few samples fall in the PM field (Figure 16a). The opposite is observed for the Bredasdorp sandstones, where about 95% of the samples are plotted in the PM (Figure 16b). Also, the calc-alkaline ($CaO–Na_2O–K_2O$), Th–Sc–Zr/10, and La–Th–Sc ternary diagrams show that majority of the Bredasdorp mudrocks and sandstones are related to PM with few contributions from the ACM (Figures 17–19). These rocks also exhibit similar geochemical characteristics with recent sedimentary rocks of East African Rift System [61], which further support a rift basin tectonic setting for the Bredasdorp Basin. The PMs are basins on continental crust and basins associated with ocean floor spreading, failed rifts, and Atlantic-type continental margins. On the other hand, ACMs are subduction related basins, continental basins, and pull-apart basins associated with strike-slip fault zones.

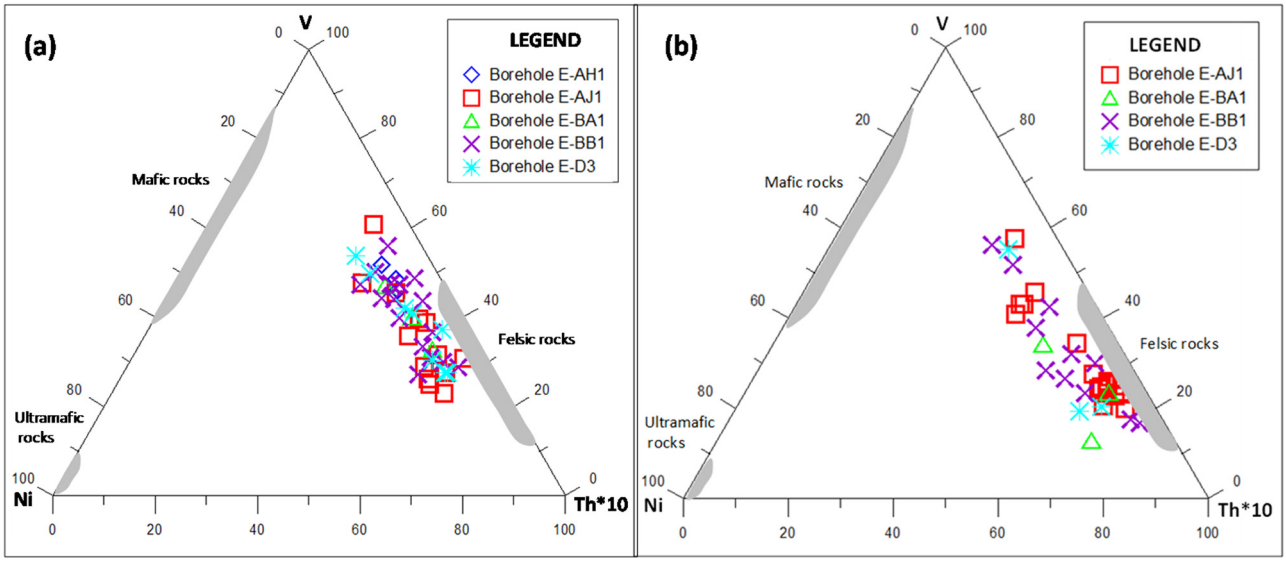

Figure 14: V-Ni-Th∗10 triangle diagram showing felsic source rock for the Bredasdorp Basin: (a) mudrocks and (b) sandstones (background field after ref. [16]).

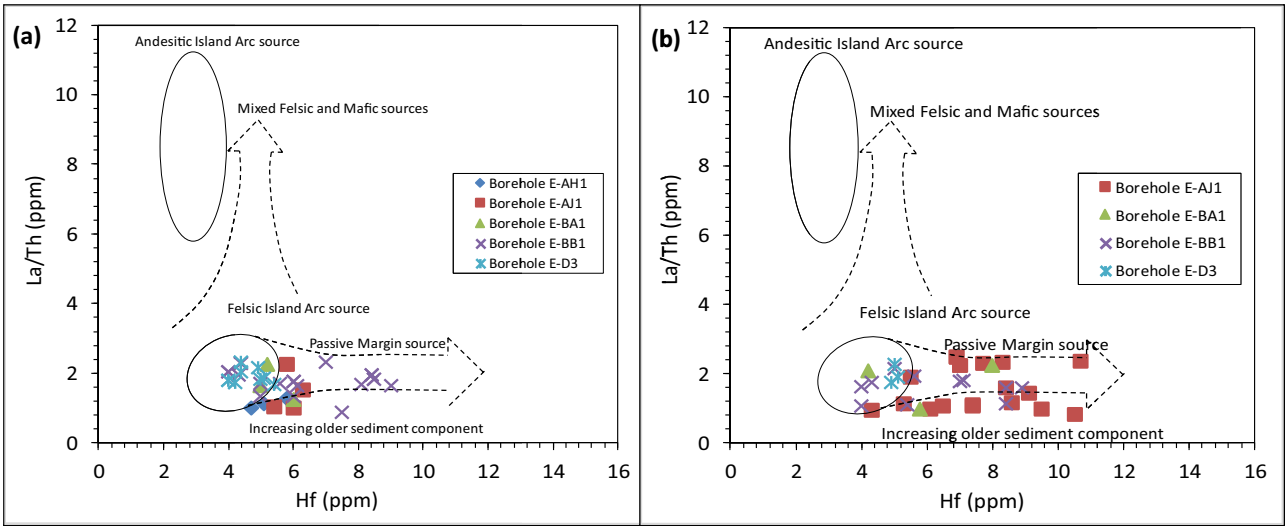

Figure 15: Bivariate plot of La/Th versus Hf showing felsic source area for the Bredasdorp Basin: (a) mudrocks and (b) sandstones (background field after ref. [57]).

5.4 Paleoweathering conditions

The degree or extent of chemical weathering of source rocks are mainly influenced by the composition of the source rock, duration of weathering, climatic conditions, and rates of tectonic uplift of source region [62]. Several researchers including [3,63,64] have reported that about 75% of labile materials in the upper crust are made up of feldspars and volcanic glass. Chemical weathering of these materials would lead to the formation of clay minerals. Elements like Ca, Na, and K are mostly removed from source rocks during chemical weathering and the amount of these elements remaining in sediments derived from the rocks serve as pointers to the degree of chemical weathering [65]. As documented by ref. [66], if clastic sedimentary rocks are free from alkali related post-depositional changes, then their alkali contents (K_2O + Na_2O) and K_2O/Na_2O ratios should be considered as good pointers to the degree of weathering of the source materials. A few indices of weathering have been proposed for the determination of the degree of source rock weathering. The indices of weathering/alteration include CIA, CIW,

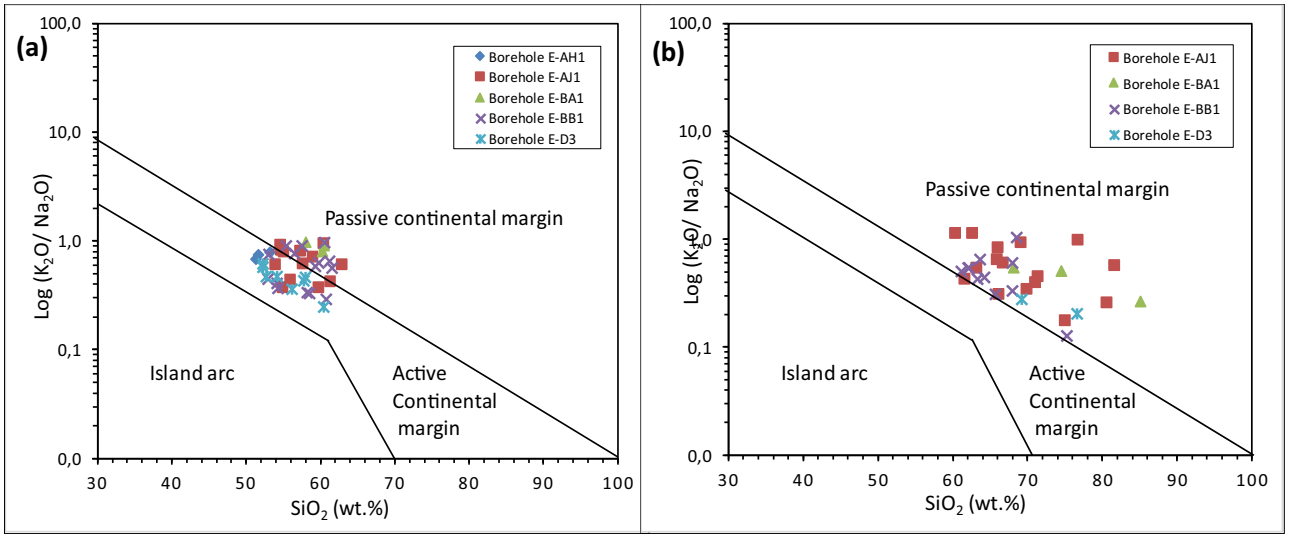

Figure 16: Binary plot of Log (K_2O/Na_2O) versus SiO_2 for Bredasdorp mudrocks showing: (a) active and passive continental settings for the mudrocks and (b) passive continental setting for the sandstones (background field after ref. [18]).

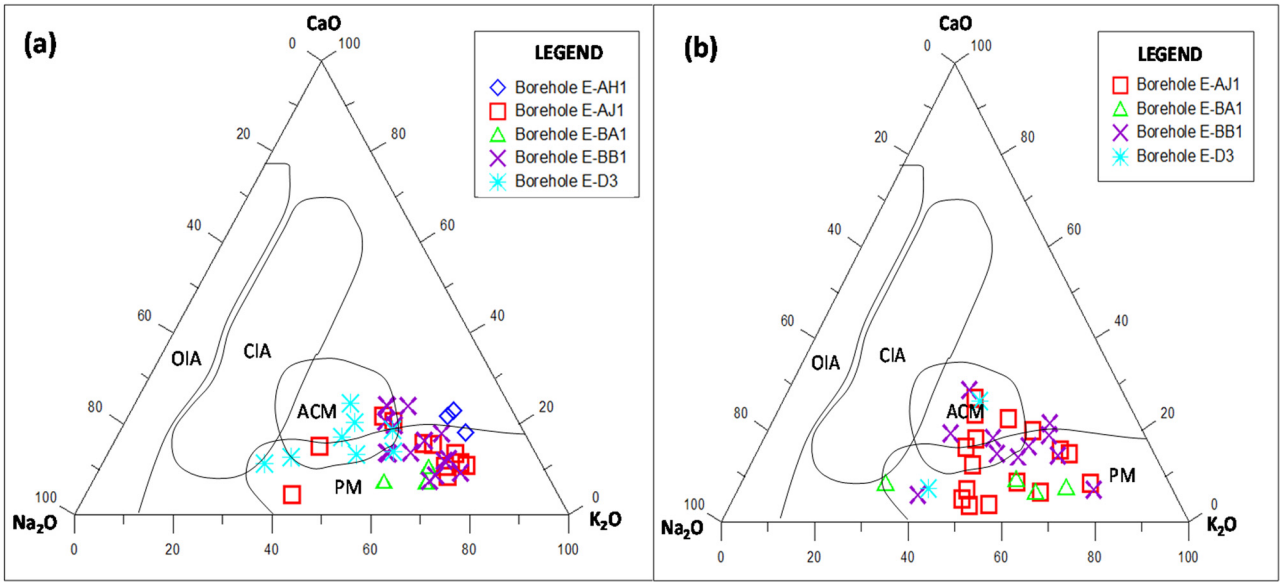

Figure 17: Na_2O–CaO–K_2O ternary plot showing active and passive continental settings for the Bredasdorp: (a) mudrocks and (b) sandstones (after ref. [59]).

and PIA. These indices are based on the molecular percentages of the mobile and immobile element oxides like Na_2O, CaO, K_2O, and Al_2O_3.

The chemical composition of the products of chemical weathering in a basin is anticipated to unravel the mobility of the surviving elements during weathering [67]. The CIA proposed in ref. [1] is the most widely used chemical index to determine the degree of source area weathering. Nesbitt and Young [1] expressed CIA as:

$$CIA = [Al_2O_3/(Al_2O_3 + CaO^* + Na_2O + K_2O)] \times 100,$$

where CaO^* is the content of CaO incorporated in silicate fraction.

The calculated indices of weathering (CIA, CIW, and PIS) are presented in the supplementary data (Table S5). The CIA is simply the ratio of primary minerals to secondary products (i.e. clay minerals). CIA values usually range from about 50 for unweathered rocks up to 100 in highly weathered rocks. Generally, CIA values increase

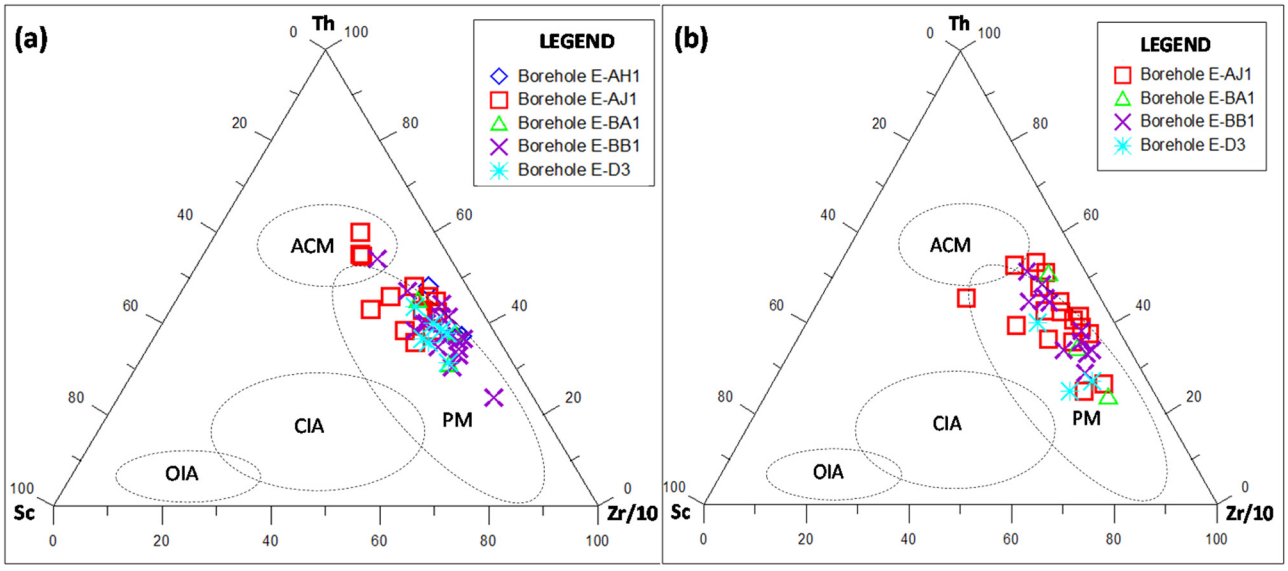

Figure 18: Th–Sc–Zr/10 ternary diagram showing: (a) active and passive continental settings for the Bredasdorp mudrocks and (b) dominance of passive continental setting for the Bredasdorp sandstones (after ref. [4]).

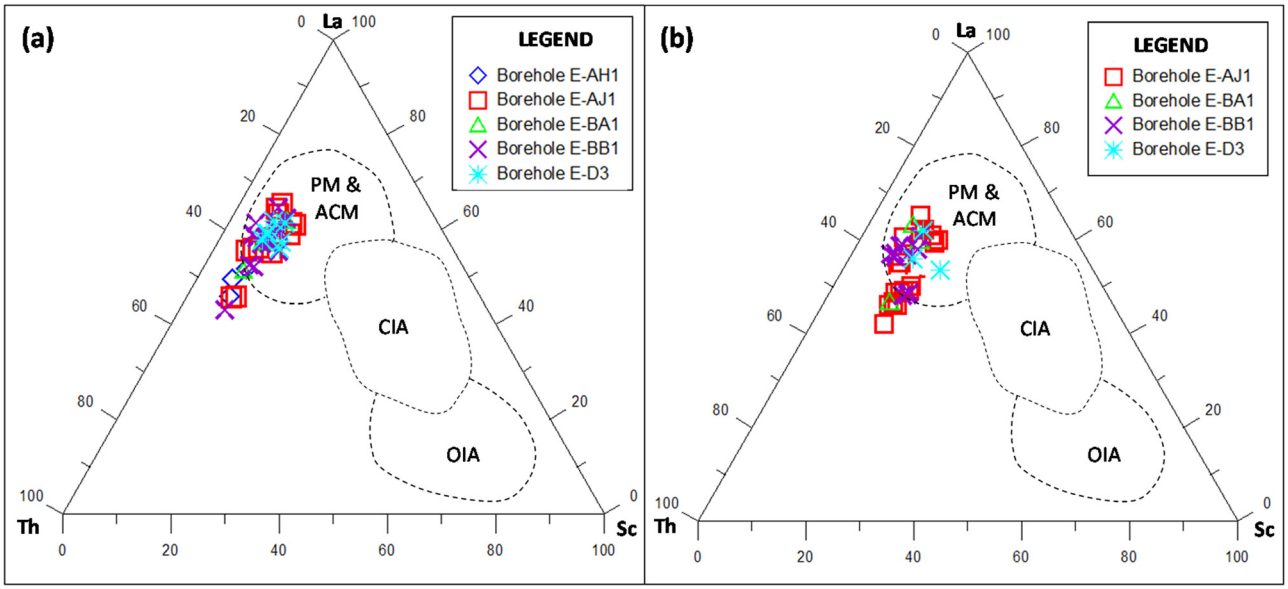

Figure 19: La–Th–Sc ternary diagram showing active and passive continental settings for the Bredasdorp: (a) mudrocks and (b) sandstones (after ref. [4]).

with the increase in the degree of weathering, reaching 100 when all the Ca, Na, and K have been leached from weathering residue. The CIA values in the Bredasdorp mudrocks and sandstones vary in the range of 82.72–86.42, 30.71–87.20, 66.31–84.01, 31.22–85.52, and 30.98–77.89 in boreholes E-AH1, E-AJ1, E-BA1, E-BB1, and E-D3, respectively. These average CIA values revealed relatively low to high degree of chemical weathering in the source area. In general, the CIA values in the mudrocks and sandstones vary from 73.50 to 90.16 and from 30.71 to 70.99, respectively. The high CIA values in the mudrocks possibly signifies the presence of clay minerals and low percentage of detrital feldspars. On the other hand, the low CIA values in the sandstones (<50%) suggest a low weathering condition in the source area and perhaps reflect cool conditions. The variations in CIA reveal changes in the properties of feldspar against aluminous clay minerals. These changes suggest that the studied samples were derived from source rocks

that have been subjected to both chemical and physical weathering.

The CIW was also calculated to reveal the degree of chemical weathering that the Bredasdorp sediments have undergone. Just like the CIA, the CIW also accounts for the rate at which feldspars are converted to clay minerals. The formula for CIW is expressed in ref. [68] as:

$$\mathrm{CIW} = [\mathrm{Al_2O_3}/(\mathrm{Al_2O_3} + \mathrm{CaO^*} + \mathrm{Na_2O})] \times 100.$$

The CIW values of the Bredasdorp mudrocks and sandstones are in the range of 93.69–94.82, 49.44–94.14, 72.32–93.97, 36.34–93.88, and 33.60–93.88 in boreholes E-AH1, E-AJ1, E-BA1, E-BB1, and E-D3, respectively. Again, the obtained CIW values indicate low to high degree of chemical weathering. The source area weathering and elemental redistribution during diagenesis of the Bredasdorp rocks were assessed using the PIA. As reported in ref. [68], the PIA records and accounts for the rate at which feldspars are progressively changed or weathered to clay minerals. The maximum value of PIA for completely weathered materials (i.e. kaolinite and gibbsite) is 100. The formula for PIA is denoted in ref. [68] as:

$$\mathrm{PIA} = [(\mathrm{Al_2O_3} - \mathrm{K_2O})/(\mathrm{Al_2O_3} + \mathrm{CaO^*} + \mathrm{Na_2O} - \mathrm{K_2O})] \times 100.$$

The PIA values of the Bredasdorp mudrocks and sandstones are in the range of 92.86–94.26, 50.33–93.75, 69.56–93.16, 31.61–91.56, and 27.46–89.60 in boreholes E-AH1, E-AJ1, E-BA1, E-BB1, and E-D3, respectively. These PIA values also signify low-high conversion rate of feldspars to clay minerals during source weathering, transport, redeposition, and diagenesis. During the preliminary stages of chemical weathering, Ca is easily leached than K and Na. As the weathering progresses, the total alkali (K_2 O+ Na_2O) content increases with the decrease in the K–Na ratio (K_2O/Na_2O), perhaps due to the destruction of feldspars; especially plagioclase ref. [24]. The feldspathic materials in the Bredasdorp mudrocks and sandstones have undergone variable degrees of weathering during the different evolution phases. As reported in ref. [24], the binary plots of K_2O/Na_2O, $K_2O + Na_2O$, Na_2O, K_2O, and CaO against PIA can unravel the mobility of elements during the final phases of chemical weathering of previously altered feldspars. These plots were also attempted for the Bredasdorp samples and it is observed (in general) that as the K_2O/Na_2O increases, the PIA also increases, whereas as $K_2O + Na_2O$ and CaO content increases, the PIA decreases (Figures 20–21). Generally, the bivariate plots show weak correlations which could be due to the presence of K-bearing minerals (i.e. muscovite and biotite) and retention of most of the mobilized K by aluminous material resulting in the formation of illite.

The Al_2O_3–(CaO + Na_2O)–K_2O (represented as A–CN–K) ternary diagram in ref. [24] is another useful approach for assessing the composition of original source rock and mobility of elements during chemical weathering of source material and post-depositional chemical modifications. The A–CN–K ternary plot of the Bredasdorp mudrocks and sandstones were plotted to unravel the compositional changes in the mudrocks and sandstones that are related to chemical weathering, diagenesis, and source rock composition. The Al_2O_3–(CaO + Na_2O)–K_2O composition of the Bredasdorp samples are plotted on the A–CN–K ternary diagram background fields of ref. [24].

The A–CN–K diagrams of the Bredasdorp samples show that about 100% of the mudrocks and 55% of the sandstones are plotted above the line joining plagioclase and K-feldspar (Figure 22). The weathering trendline of the Bredasdorp shales is closer to the A–K boundary, signifying that the silicates (i.e. feldspar) have experienced intense or high weathering resulting in the leaching of Ca and Na out of plagioclase. In addition, the trendline (red arrow in Figure 22) parallels with the A–K boundary and slightly extend towards the A apex, signifying leaching of K and enrichment of Al. This indicates that further weathering has led to the decomposition of K-bearing minerals (biotite, illite, and potassium feldspar). Thus, kaolinite dominates the secondary clay minerals. On the other hand, the weathering trendline of the Bredasdorp sandstones is relatively closer to the A–CN boundary, indicating that plagioclase are the first to be weathered, out of which Ca and Na leached rapidly, whereas K-feldspar is relatively stable. In the sandstones, illite and smectite are the main weathering products, whereas kaolinite did not dominate. Samples with CIA values below 50 are unweathered.

5.5 Sediment maturity and climatic conditions

The maturity of sediments and paleoclimatic conditions can be determined by computing the ICV suggested in ref. [69]. The ICV values tend to be high in minerals that underwent intensive degree of weathering and low in less weathered or more stable minerals. As reported in ref. [69], ICV values generally decrease further in the montmorillonite group of clay minerals and are lowest in the kaolinite group minerals. Furthermore, mudrocks and sandstones that have ICV value of less than 1 are compositionally mature and are deposited in the tectonically quiescent or cratonic environment where sediment

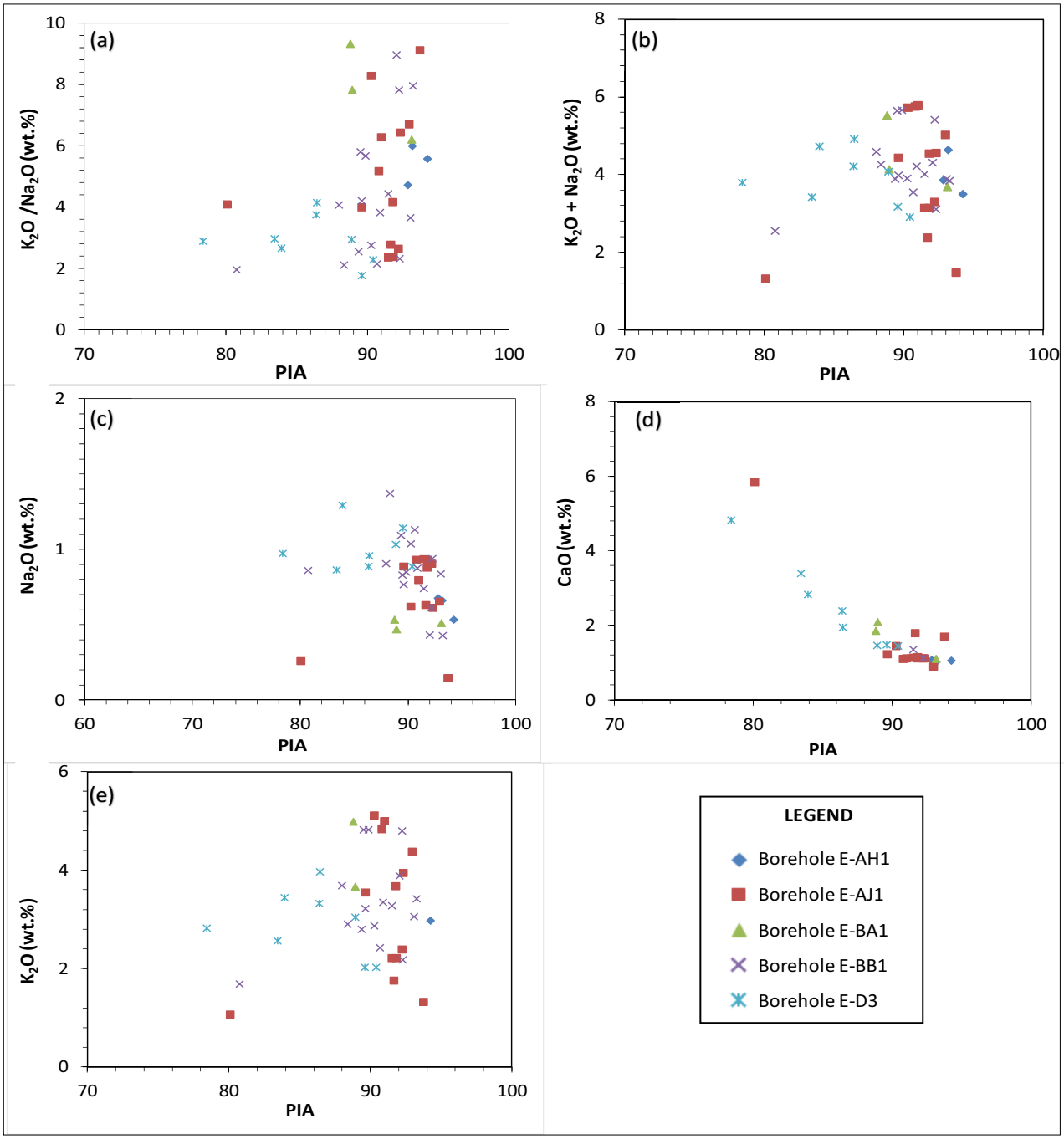

Figure 20: Bivariate diagrams depicting mobility of elements during weathering of feldspars in the Bredasdorp shales: (a) (K_2O/Na_2O) wt% versus PIA, (b) (K_2O + Na_2O) wt% versus PIA, (c) Na_2O wt% versus PIA, (d) CaO wt,% versus PIA, and (e) K_2O wt% versus PIA.

recycling is active. In contrast, mudrocks and sandstones that have ICV value of greater than 1 are compositionally immature with the first cycle of sediments deposited in tectonically active settings. The ICV formula is presented in ref. [69] as:

$$ICV = (Fe_2O_3 + K_2O + Na_2O + CaO + MgO + MnO)/Al_2O_3.$$

The ICV values for the Bredasdorp mudrocks vary from 0.23 to 0.61, averaging 0.43, whereas ICV values for the sandstones range from 0.71 to 3.75, averaging 2.82. In fact, only 4 out of the 26 sandstone samples have ICV of less than 1. Based on the average ICV values, it can be inferred that the shales are compositionally mature, while the sandstones are compositionally

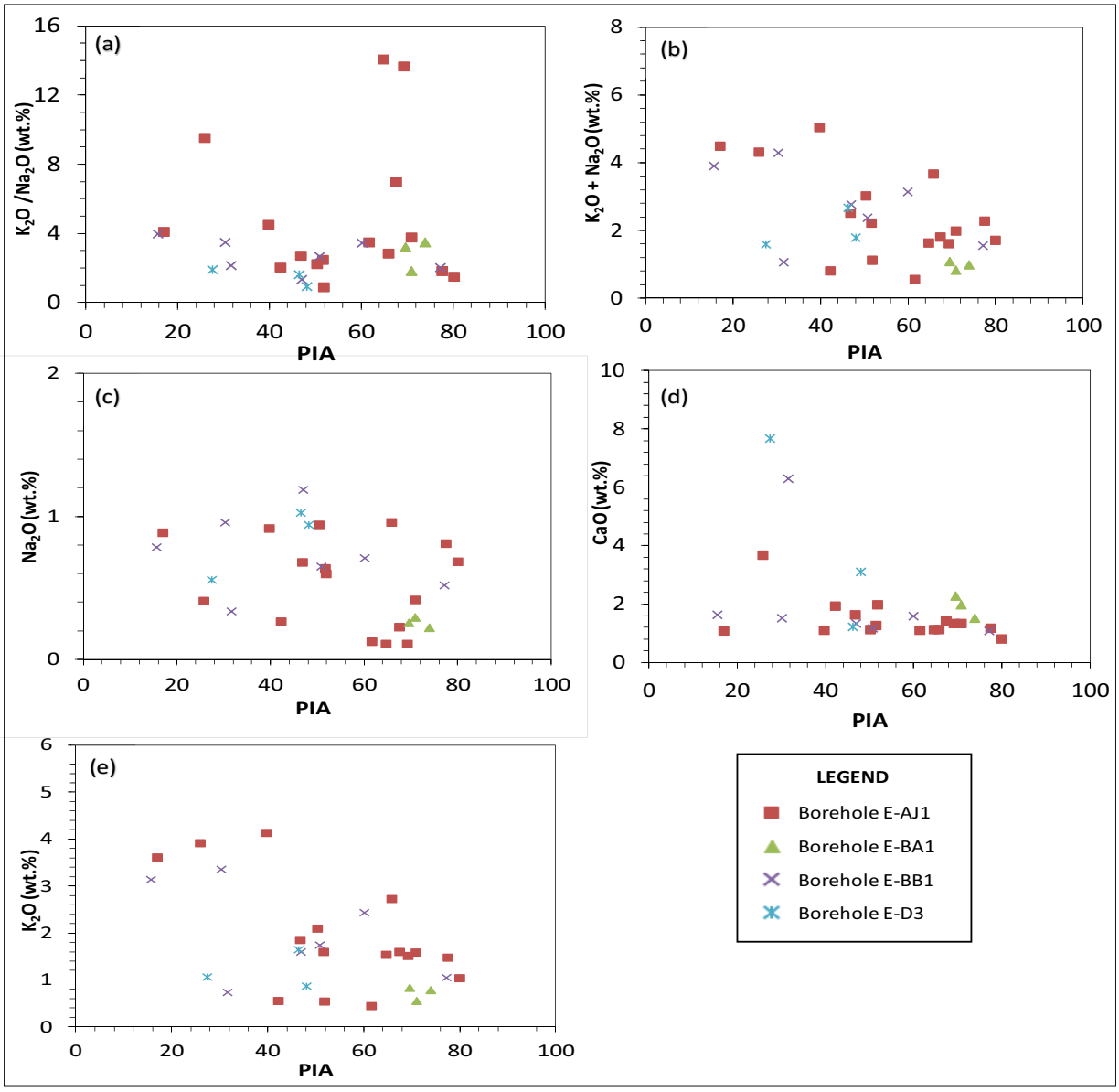

Figure 21: Bivariate diagrams depicting mobility of elements during weathering of feldspars in the Bredasdorp sandstones: (a) (K_2O/Na_2O) wt% versus PIA, (b) ($K_2O + Na_2O$) wt% versus PIA, (c) Na_2O wt% versus PIA, (d) CaO wt% versus PIA, and (e) K_2O wt% versus PIA.

immature with the first cycle of sediments deposited in tectonically active settings. The bivariate plot of CIA versus ICV for the Bredasdorp rocks shows that the shales are geochemically mature and are derived from intensively weathered source rocks, whereas the sandstones are geochemically immature and derived from weak weathered source rocks (Figure 23). To constrain the climatic condition during sedimentation of clastic sedimentary rocks, the plot of SiO_2 against (Al_2O_3 + K_2 O+ Na_2O) proposed in ref. [70] was used to classify the maturity of Bredasdorp mudrocks and sandstones as a function of climate. The binary plot of SiO_2 versus (Al_2O_3 + K_2 O+ Na_2O) shows that the mudrocks are of arid climates, while the sandstones are of humid climate with varied maturities (Figure 24).

6 Conclusion

The provenance, tectonic setting, and paleoweathering conditions of the Cretaceous mudrocks and sandstones from the Bredasdorp Basin have been assessed using inorganic geochemical studies. On the basis of the major oxide compositions, the sandstones could be classified as

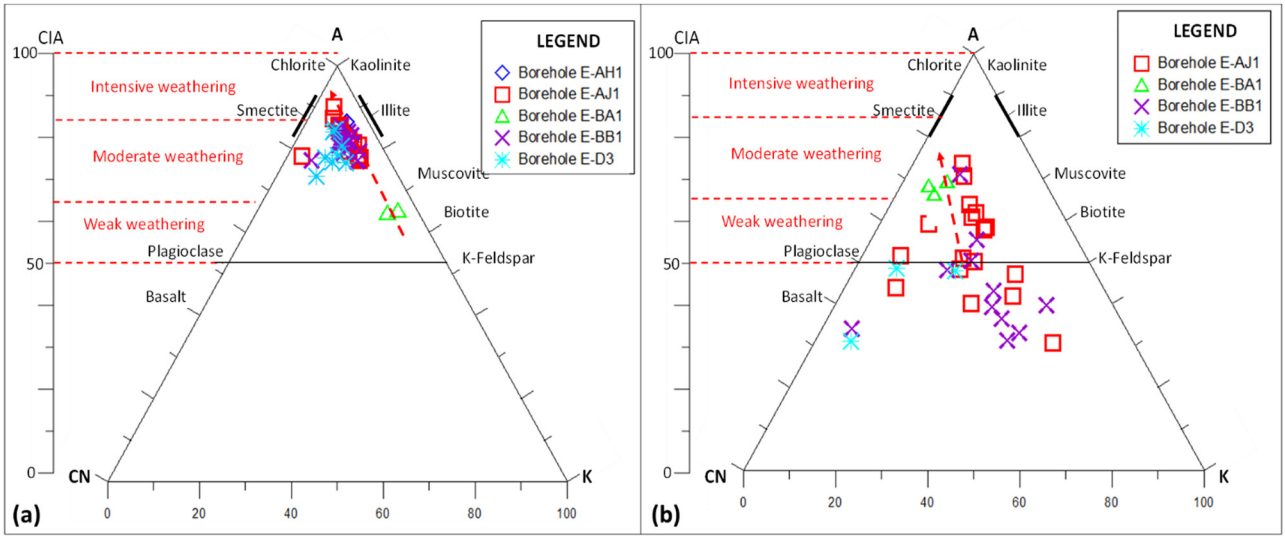

Figure 22: A–CN–K ternary diagram of molecular proportions of Al_2O_3-(CaO + Na_2O)-K_2O for the Bredasdorp: (a) mudrocks and (b) sandstones (background field after ref. [24]). The CIA scale shown at the left side is for comparison.

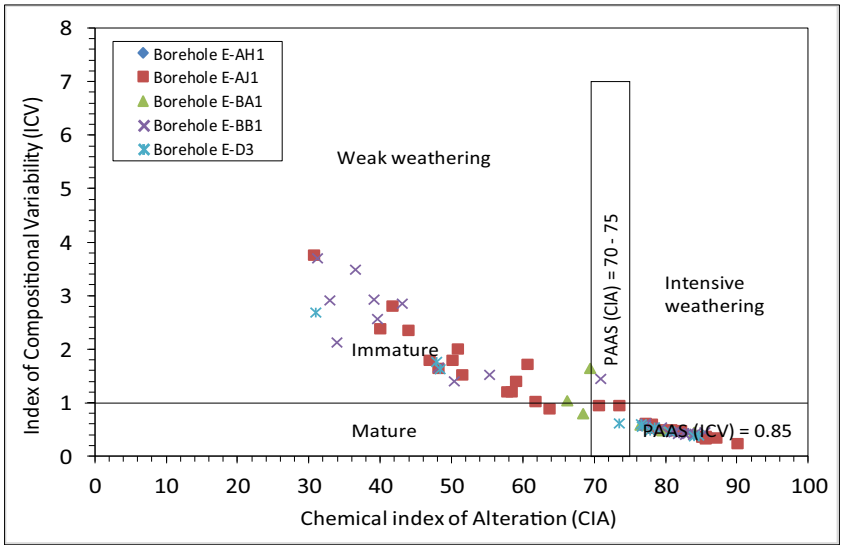

Figure 23: Binary plot of CIA against ICV for the Bredasdorp mudrocks and sandstones.

sub-arkose and sub-lithic arenite. The major oxide and trace element concentrations in the mudrocks and sandstones show significant variation in composition across the samples. Higher concentrations of Al_2O_3, Fe_2O_3, K_2O, Sc, V, Zr, Th, U, La, Ce, and Ni are observed in the mudrocks than the sandstones, whereas the sandstones are enriched with SiO_2, Hf, Cr, and Zn than the mudrocks. The preferential enrichment of transitional elements like Sc, V, and Ni in the mudrocks is probably due to the surficial sorption. Furthermore, the low concentration of these elements, La/Sc ratio, and Th/Sc ratio suggest the presence of fractionated source rocks with lower compatible element contents and recycled sediments in the source area. Likewise, the discrimination diagrams based on major oxide geochemistry shows that the sediments are mainly of quartzose sedimentary provenance with little contribution from the intermediate igneous provenance, suggesting that they were mostly derived from a cratonic interior or recycled orogen. The tectonic setting discrimination diagrams support PM-ACM setting of the provenance. In addition, the closely similar geochemical compositions of the analysed samples and recent sedimentary rocks of the East African Rift System suggest a rifted basin tectonic setting for the Bredasdorp Basin. The

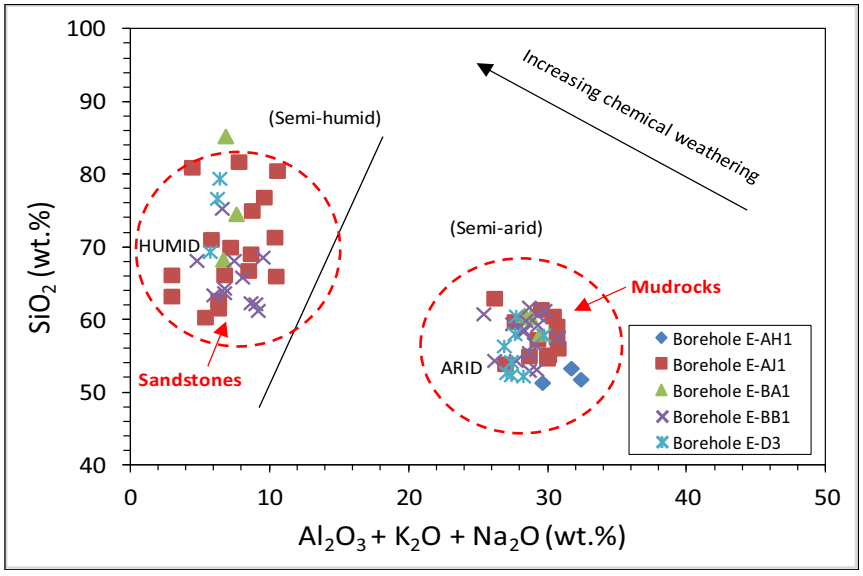

Figure 24: Chemical maturity of the Bredasdorp mudrocks and sandstones (background field after ref. [70]).

CIA and PIA values, as well as the bivariate plots of ICV versus CIA, and SiO_2 against total alkali (Al_2O_3 + K_2O + Na_2O) suggest that the source area of the Bredasdorp mudrocks and sandstones were subjected to low and intense weathering conditions under arid and humid climate, respectively.

Acknowledgments: The authors are grateful to the National Research Foundation-Southern African Systems Analysis Centre (NRF-SASAC) and the DSI-NRF Centre of Excellence (CoE) for Integrated Mineral and Energy Resource Analysis (CIMERA) for financial support. The Petroleum Agency of South Africa (PASA) and the Govan Mbeki Research and Development Centre (GMRDC) of the University of Fort Hare are appreciated for granting access to the cores and logistic supports, respectively.

Funding information: National Research Foundation-Southern African Systems Analysis Centre (NRF-SASAC) and the DSI-NRF Centre of Excellence (CoE) for Integrated Mineral and Energy Resource Analysis (CIMERA).

Conflict of interest: The authors declared that there is no actual or potential conflict of interest including any financial, personal, or other relationships with other people or organizations regarding the publication of this original manuscript.

References

[1] Nesbitt HW, Young GM. Early Proterozoic climates and plate motions inferred from major element chemistry of lutites. Nature. 1982;299:715–7.

[2] Raza M, Dayal AM, Khan A, Bhardwaj VR, Rais S. Geochemistry of lower Vindhyan clastic sedimentary rocks of North-western Indian shield: implications for composition and weathering history of Proterozoic continental crust. J Asian Earth Sci. 2010;39:51–61.

[3] Taylor SR, McLennan SM. The continental crust: its composition and evolution. Oxford, England: Blackwell Scientific Publications; 1985. p. 275–93.

[4] Bhatia MR, Crook KAW. Trace element characteristics of greywacke and tectonic setting discrimination of sedimentary basins. Contrib Mineral Petrol. 1986;92:181–93.

[5] Cullers RL, Barrett T, Carlson R, Robinson B. Rare earth element and mineralogical changes in Holocene soil and stream sediment: a case study in the Wet Mountains, Colorado, USA. Chem Geol. 1987;63:275–97.

[6] Cullers RL, Basu A, Suttner L. Geochemical signature of provenance in sand-size material in soils and stream sediments near the Tobacco Root batholith, Montana, USA. Chem Geol. 1988;70:335–48.

[7] McLennan SM, Hemming S, McDaniel DK, Hanson GN. Geochemical approaches to sedimentation, provenance and tectonics. In: Johnson MJ, Basu A, editors. Processes Controlling the Composition of Clastic Sediments Geological Society of American Special Paper; 1993. p. 21–40.

[8] Wronkiewicz DJ, Condie KC. Geochemistry and mineralogy of sediments from the Ventersdorp and Transvaal Supergroups,

South Africa: cratonic evolution during the early Proterozoic. Geochim Cosmochim Acta. 1990;54:343–54.
[9] Umazano AM, Bellosi ES, Visconti G, Jalfin AG, Melchor RN. Sedimentary record of a late Cretaceous volcanic arc in central Patagonia: petrography, geochemistry and provenance of fluvial volcaniclastic deposits of the Bajo Barreal formation, San Jorge Basin, Argentina. Cretac Res. 2009;30:749–66.
[10] Fanti F. Bentonite chemical features as proxy of late Cretaceous provenance changes: a case study from the Western interior Basin of Canada. Sediment Geol. 2009;217:112–27.
[11] Baiyegunhi C, Liu K, Gwavava O. Geochemistry of sandstones and shales from the Ecca group, in the Eastern Cape Province of South Africa: implication for provenance and tectonic setting. Open Geosci. 2017;9:340–60.
[12] Pettijohn FJ. Sedimentary rocks. 3rd edn. New York: Harper and Row; 1975. p. 628
[13] McCulloch MT, Wasserburg GJ. Sm-Nd and Rb-Sr chronology of continental crust formation. Science. 1978;200:1003–11.
[14] Condie KC. Chemical composition and evolution of the upper continental crust: contrasting results from surface samples and shales. Chem Geol. 1993;104:21–37.
[15] McLennan SM, Simonetti A, Goldstein SL. Nd and Pb isotopic evidence for provenance and post-depositional alteration of the Paleoproterozoic Huronian Supergroup, Canada. Precambrian Res. 2000;102:263–78.
[16] Bracciali L, Marroni M, Pandolfi L, Rocchi S. Geochemistry and petrography of Western Tethys Cretaceous sedimentary covers (Corsica and Northern Apennines): from source area to configuration of margins. In: Arribas J, Critlli S, Johanson MJ, editors. Sedimentary provenance and petrogenesis: Perspectives from petrography and geochemistry: Geological Society of America, Special Paper 420; 2007. p. 73–93.
[17] Bhatia MR. Plate tectonics and geochemical composition of sandstones. J Geol. 1983;91:611–27.
[18] Roser BP, Korsch RJ. Determination of tectonic setting of sandstone-mudstone suites using SiO_2 content and K_2O/Na_2O ratio. J Geol. 1986;94:635–50.
[19] McLennan SM, Taylor SR, Eriksson KA. Geochemistry of Archaean shales from the Pilbara supergroup, Western Australia. Geochim Cosmochim Acta. 1983;47(7):1211–22.
[20] Hayashi K, Fujisawa H, Holland H, Ohmoto H. Geochemistry of ~1.9 Ga sedimentary rocks from north-eastern Labrador, Canada. Geochimica et Cosmochimica Acta. 1977;61(19):4115–37.
[21] Nesbitt HW. Petrogenesis of siliciclastic sediments and sedimentary rocks. In: Lenz DR, editor. Geochemistry of sediments and sedimentary rocks. Newfoundland: Geologists Association of Canada, Geotext 4; 2003. p. 39–51.
[22] Huntsman-Mapila P, Mumpunzu AB, Vink B, Ringrose S. Cryptic indicators of provenance from the geochemistry of the Okavango Delta sediments, Botswana. Sediment Geol. 2005;174:123–48.
[23] Weaver CE. Clays, muds and shales. Amsterdam: Elsevier; 1989. p. 671–88.
[24] Nesbitt HW, Young GM. Prediction of some weathering trends of plutonic and volcanic rocks based upon thermodynamic and kinetic consideration. Geochimica et Cosmochimica Acta. 1984;48:1523–34.
[25] McLennan SM, Taylor SR, McCulloch MT, Maynard JB. Geochemical and Nd-Sr isotopic composition of deep sea turbidites: Crustal evolution and plate tectonic associations. Geochim Cosmochim Acta. 1990;54:2015–50.
[26] Armstrong-Altrin JS, Lee YI, Verma SP, Ramasamy S. Geochemistry of sandstones from the upper Miocene Kudankulam formation, southern India: implication for provenance, weathering and tectonic setting. J Sediment Res. 2004;74:285–97.
[27] Lee JI, Park BK, Jwa YJ, Yoon HI, Yoo KC, Kim Y. Geochemical characteristics and the provenance of sediments in the Bransfield Strait, West Antarctica. Mar Geol. 2005;219:81–98.
[28] Wanas HA, Abdel-Maguid NM. Petrography and geochemistry of the Cambro–Ordovician Wajid Sandstone, southwest Saudi Arabia: implications for provenance and tectonic setting. J Asian Earth Sci. 2006;26:1–14.
[29] Dickinson WR, Beard LS, Brakenridge GR, Erjavec JL, Ferguson RG, Inman KF, et al. Provenance of North Phanerozoic sandstones in relation to tectonic setting. Geol Soc Am Bull. 1983;94:222–35.
[30] Critelli S, Ingersoll RV. Interpretation of neovolcanic versus paleovolcanic sand grains: an example from Miocene deep marine sandstones of the Topanga Group (southern California). Sedimentology. 1995;42:783–804.
[31] Cullers RL, Podkovyrov VL. Geochemistry of the mesoproterozoic Lakhanda shales in southeastern Yakutia, Russia: implications for mineralogical and provenance control and recycling. Precambrian Res. 2000;104:77–93.
[32] Burden PLA, Davies CPN. Exploration to first production on block 9 off South Africa. Oil Gas J. 1997;1:92–8.
[33] Akinlua A, Sigedle A, Buthelezi T, Fadipe OA. Trace element geochemistry of crude oils and condensates from South African Basins. Mar Pet Geol. 2015;59:286–93.
[34] Sonibare WA. Structure and evolution of basin and petroleum systems within a transform- related passive margin setting: data-based insights from crust-scale 3D modelling of the Western Bredasdorp Basin, offshore South Africa. PhD. Thesis. Cape Town: University of Stellenbosch; 2015. p. 294.
[35] McMillan IK, Brink GJ, Broad DS, Maier JJ. Late Mesozoic sedimentary basins off the south coast of South Africa. In: Selley RC, editor. Sedimentary basins of the world—African basins. Amsterdam: Elsevier Science B.V; 1997. p. 319–76.
[36] Petroleum Agency South Africa, PASA. Petroleum exploration information and opportunities: Petroleum Agency South Africa brochure; 2005. p. 16–18.
[37] Petroleum Agency South Africa, PASA. Petroleum exploration in South Africa, information and opportunities. Online Report, Cape Town; 2012. p. 25–29. http://www.petroleumagencysa.com/images/pdfs/pet_expl_opp_2012fw.pdf
[38] Burden PLA. Soekor, partners explore possibilities in Bredasdorp Basin off South Africa. Oil Gas Jour. 1992; 90/51:109–12.
[39] Jungslager EHA. Geological evaluation of the remaining prospectivity for oil and gas of the Pre-1At1 "Synrift" succession in Block 9, Republic of South Africa. Unpublished Soekor Technical Report SOE-EXP-RPT-0380; 1996. p. 63.
[40] Broad DS, Jungslager EHA, McLachlan IR, Roux J. Offshore Mesozoic basins. In: Johnson MR, Anhaeusser CR, Thomas RJ, editors. The Geology of South Africa. Pretoria: Geological

Society of South Africa, Johannesburg/Council for Geoscience; 2006. p. 553–71.
[41] PGS. Re-evaluation of the F-A Field and Satellite. Revision. Unpublished. Cape Town; 1999. p. 57.
[42] Petroleum Agency South Africa, PASA. Western Bredasdorp. Cape Town, South Africa; Basin: Petroleum Agency South Africa Brochure; 2009. p. 13–16.
[43] Bock B, McLennan SM, Hanson GN. Geochemistry and provenance of the Middle Ordovician Austin Glen Member (Normanskill formation) and the Taconian Orogeny in New England. Sedimentology. 1998;45:635–55.
[44] Pettijohn FJ. Sedimentary rocks. 2nd edn. New York: Harper and Row; 1957. p. 718
[45] Turekan KK, Wedephol KH. Distribution of the elements in some major units of the Earth's crust. Geol Soc Am Bull. 1961;72:175–91.
[46] Gromet LP, Dymek RF, Haskin LA, Korotev RL. The North American shale composite. Its compilation, major and trace element characteristics. Geochim Cosmochim Acta. 1984;48:2469–82.
[47] Bauluz B, Mayayo MJ, Fernandez-Nieto C, Gonzalez-Lopez JM. Geochemistry of Precambrian and Paleozoic siliciclastic rocks from the Iberian Range (NE Spain): implications for source-area weathering, sorting, provenance, and tectonic setting. Chem Geol. 2000;168:135–50.
[48] Rudnick RL, Gao S. Composition of the continental crust. Treatise Geochem. 2003;3:1–64.
[49] Das BK, AL-Mikhlafi AS, Kaur P. Geochemistry of Mansar Lake sediments, Jammu, India: Implication for source-area weathering, provenance, and tectonic setting. J Asian Earth Sci. 2006;26:649–68.
[50] Levinson AA. Introduction exploration geochem. Illnois: Applied Publishing; 1974. p. 34.
[51] Vine JD, Tourtelot EB. Geochemistry of black shale deposits - a summary report. Econ Geol. 1970;65:253–72.
[52] Bauluz B, Nieto F, Mata P, Giorgetti G, Arkai P, Peacor D. Retrograde diagenesis: a widespread process on a regional scale. Clay Miner. 2005;1:93–104.
[53] Pettijohn FJ, Potter PE, Siever R. Sand and Sandstone. New York: Springer; 1987. p. 553
[54] Herron MM. Geochemical classification of terrigenous sands and shales from core or log data. J Sediment Petrology. 1988;58:820–9.
[55] Roser BP, Korsch RJ. Provenance signature of sandstone mudstone suite determined using discriminant function analysis of major element data. Chem Geol. 1988;67:119–39.
[56] Floyd PA, Winchester JA, Park RG. Geochemistry and tectonic setting of Lewisian clastic metasediments from the early Proterozoic Loch Maree group of Gairloch, N.W. Scotland. Precambrian Res. 1989;45(1–3):203–14.
[57] Floyd PA, Leveridge BE. Tectonic environment of the Devonian Gramscatho basin, south Cornwall: framework mode and geochemical evidence from turbiditic sandstones. J Geol Soc Lond. 1987;144:531–42.
[58] McCann T. Petrological and geochemical determination of provenance in the southern Welsh Basin. In: Morton AC, Todd SP, Haughton PDW, editors. Developments in sedimentary provenance. Vol. 57. London, UK: Geological Society Special Publication; 1991. p. 215–30.
[59] Toulkeridis T, Clauer N, Kröner A, Reimer T, Todt W. Characterization, provenance, and tectonic setting of Fig Tree greywackes from the Archaen Barberton Greenstone Belt, South Africa. Sediment Geol. 1999;124:113–29.
[60] Murphy JB. Tectonic influence on sedimentation along the southern flank of the late Paleozoic Magdalen basin in the Canadian Appalachians: Geochemical and isotopic constrains on the Horton Group in the St. Marys basin, Nova Scotia. Geol Soc Am Bull. 2000;112:997–1011.
[61] Mapila-huntsman P, Teircelin J-J, Benoit M, Ringrose S, Diskin S, Cotton J, et al. Sediment geochemistry and tectonic setting: application of discrimination diagrams to early stages of intracontinental rift evolution, with examples from the Okavango and Southern Tanganyika rift basins. J Afr Earth Sci. 2009;53:33–44.
[62] Wronkiewicz DJ, Condie KC. Geochemistry of Archean shales from the Witwatersrand Supergroup, South Africa: source-area weathering and provenance. Geochim Cosmochim Acta. 1987;51:2401–16.
[63] Nesbitt HW, Young GM. Formation and diagenesis of weathering profiles. J Geol. 1989;97:129–47.
[64] Fedo CM, Nesbitt HW, Young GM. Unravelling the effects of potassium metasomatism in sedimentary rocks and paleosols, with implications for paleoweathering conditions and provenance. Geology. 1995;23:921–4.
[65] Nesbitt HW, Fedo CM, Young GM. Quartz and feldspar stability, steady and non-steady state weathering and petrogenesis of siliciclastic sands and muds. J Geol. 1997;105:173–91.
[66] Lindsey DA. An evaluation of alternative chemical classifications of sandstones. USGS Open File Report; 1999. p. 1–23.
[67] Singh KP. Non-linear estimation of aquifer parameters from surficial resistivity measurements. Hydrol Earth Syst Sci Discuss. 2005;2:917–38.
[68] Harnois L. The CIW index: a new chemical index of weathering. Sediment Geol. 1988;55(3–4):319–22.
[69] Cox R, Low DR, Cullers RL. The influence of sediment recycling and basement composition on evolution of mudrock chemistry in the south-western United States. Geochim Cosmochim Acta. 1995;59(14):2919–40.
[70] Suttner LJ, Dutta PK. Alluvial sandstone composition and palaeoclimate: I. Framework mineralogy. J Sediment Petrol. 1986;56:329–45.

Appendix

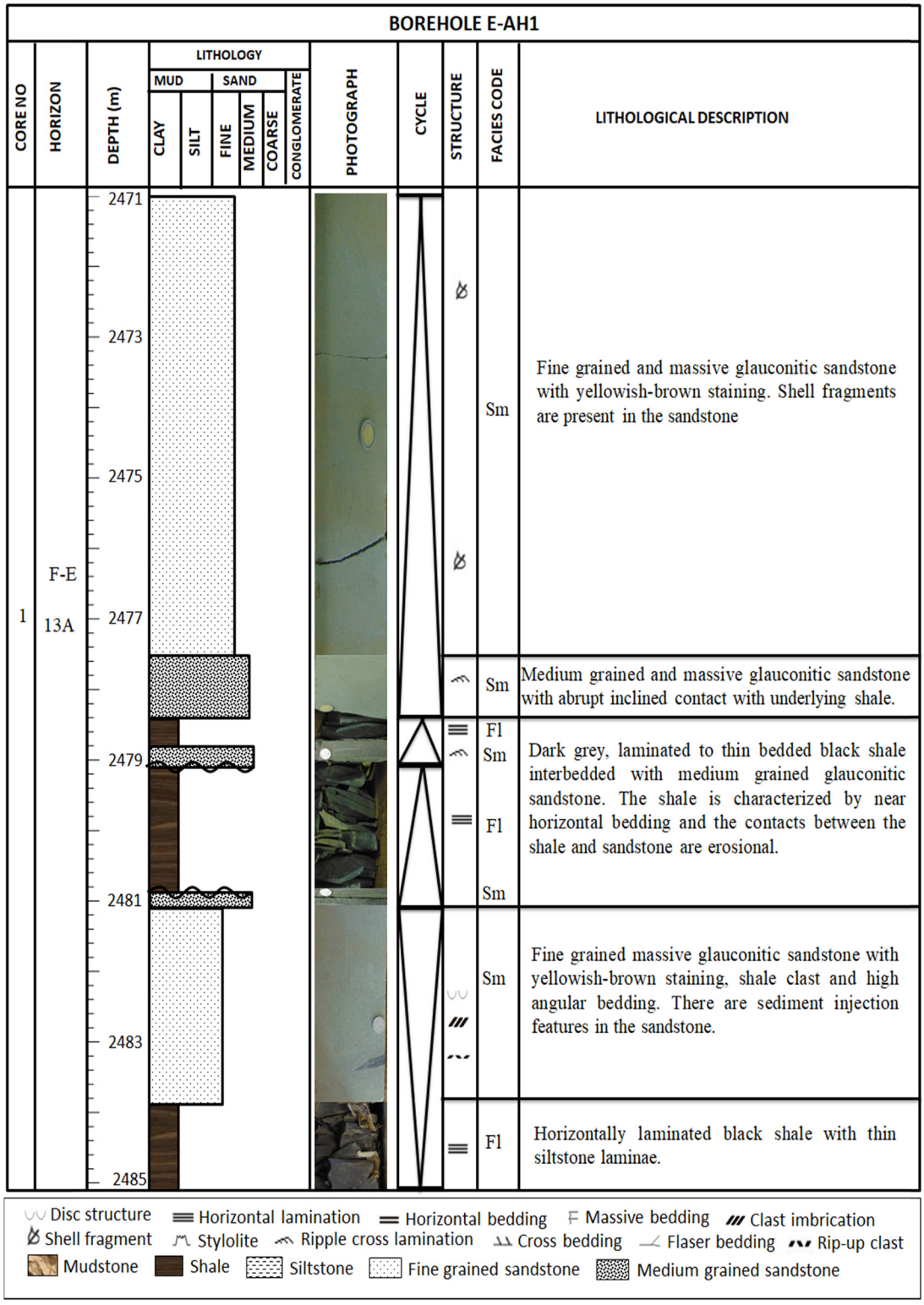

(*Continued*)

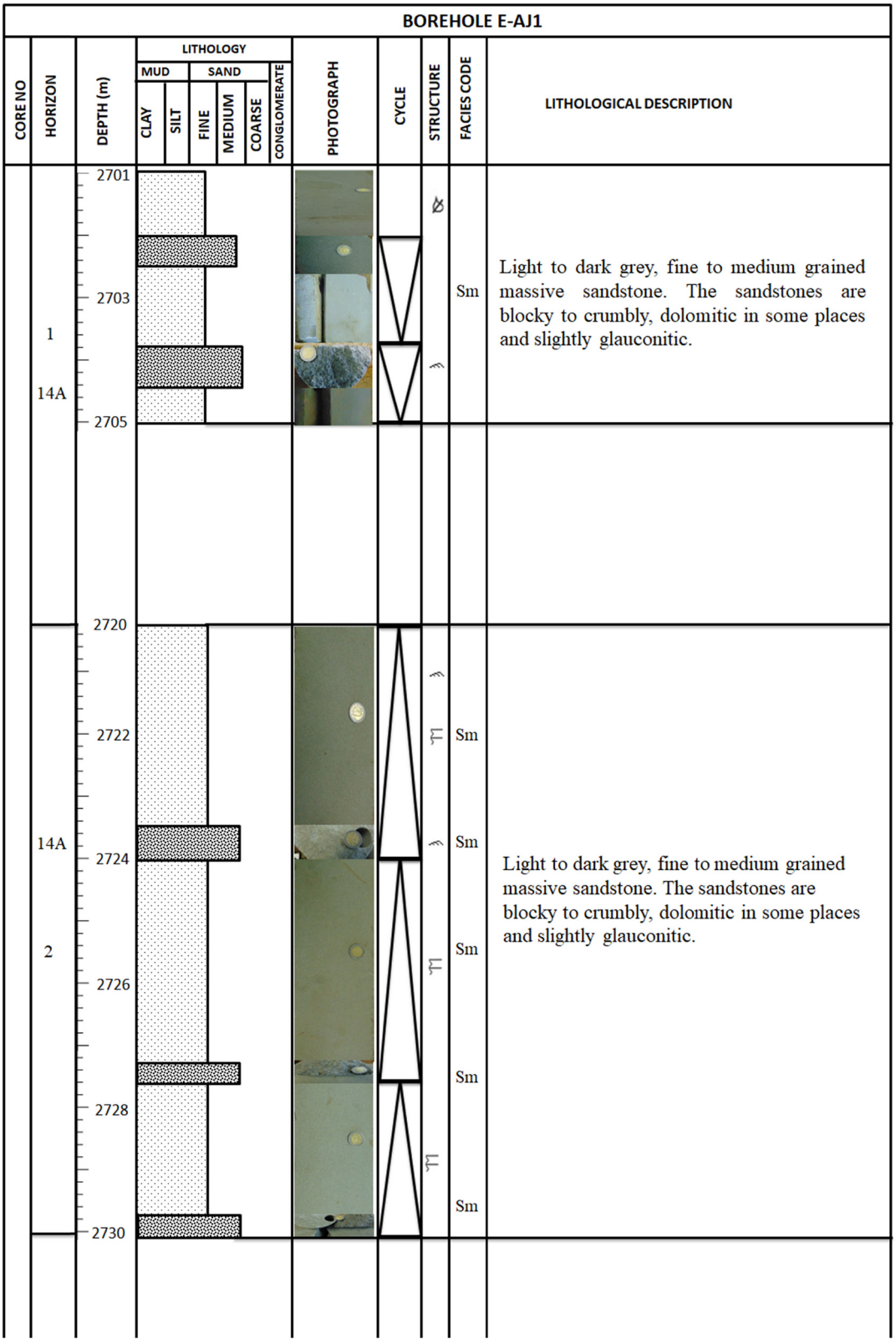
BOREHOLE E-AJ1
CORE NO
HORIZON
DEPTH (m)
LITHOLOGY
MUD
SAND
CLAY
SILT
FINE
MEDIUM
COARSE
CONGLOMERATE
PHOTOGRAPH
CYCLE
STRUCTURE
FACIES CODE
LITHOLOGICAL DESCRIPTION
2701
2703
2705
2720
2722
2724
2726
2728
2730
1
14A
14A
2
Sm
Sm
Sm
Sm
Sm
Light to dark grey, fine to medium grained massive sandstone. The sandstones are blocky to crumbly, dolomitic in some places and slightly glauconitic.
Light to dark grey, fine to medium grained massive sandstone. The sandstones are blocky to crumbly, dolomitic in some places and slightly glauconitic.

(*Continued*)

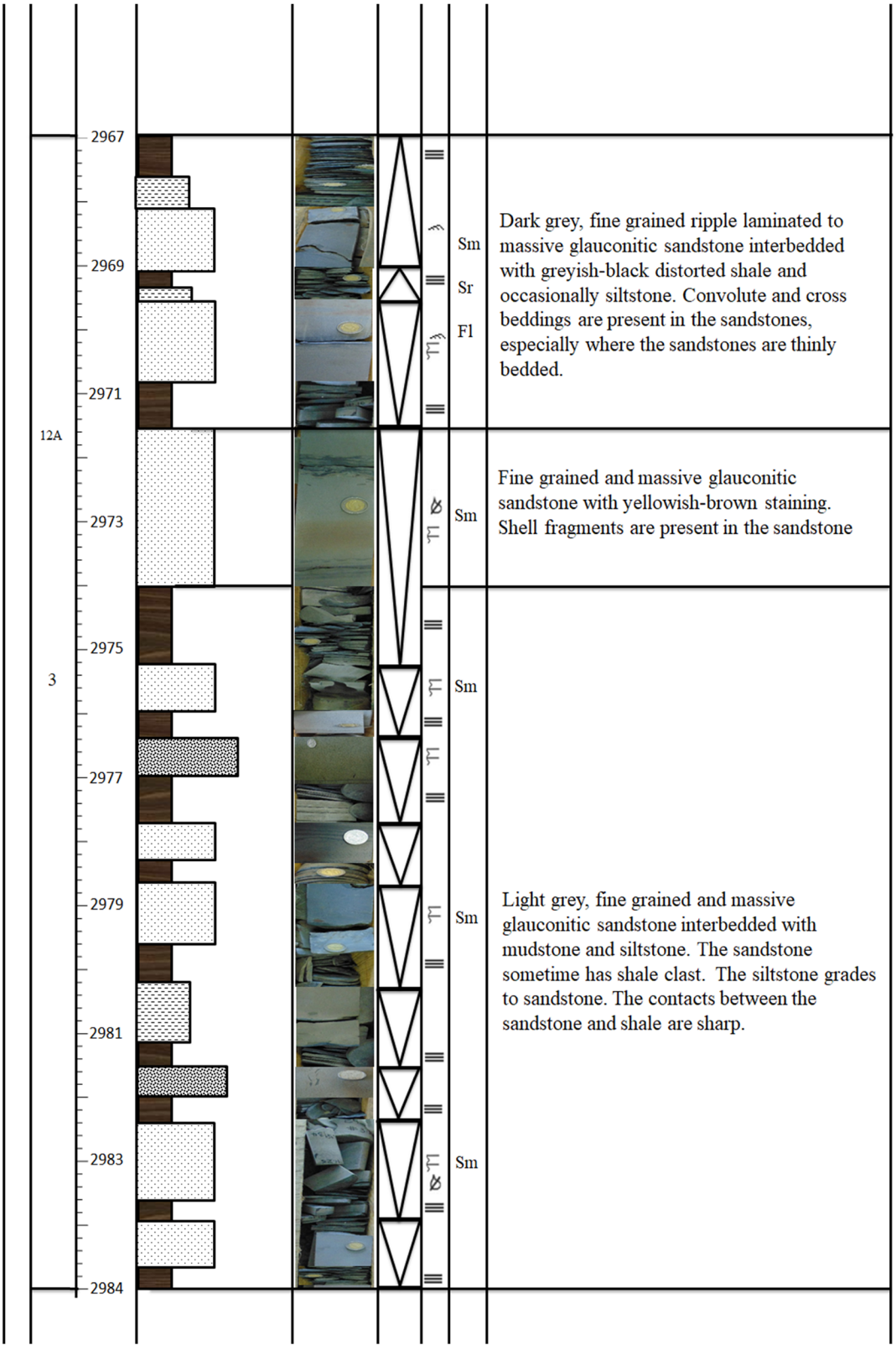
2967
2969
2971
2973
2975
2977
2979
2981
2983
2984
12A
3
Sm
Sr
Fl
Sm
Sm
Sm
Sm
Dark grey, fine grained ripple laminated to massive glauconitic sandstone interbedded with greyish-black distorted shale and occasionally siltstone. Convolute and cross beddings are present in the sandstones, especially where the sandstones are thinly bedded.
Fine grained and massive glauconitic sandstone with yellowish-brown staining. Shell fragments are present in the sandstone
Light grey, fine grained and massive glauconitic sandstone interbedded with mudstone and siltstone. The sandstone sometime has shale clast. The siltstone grades to sandstone. The contacts between the sandstone and shale are sharp.

(*Continued*)

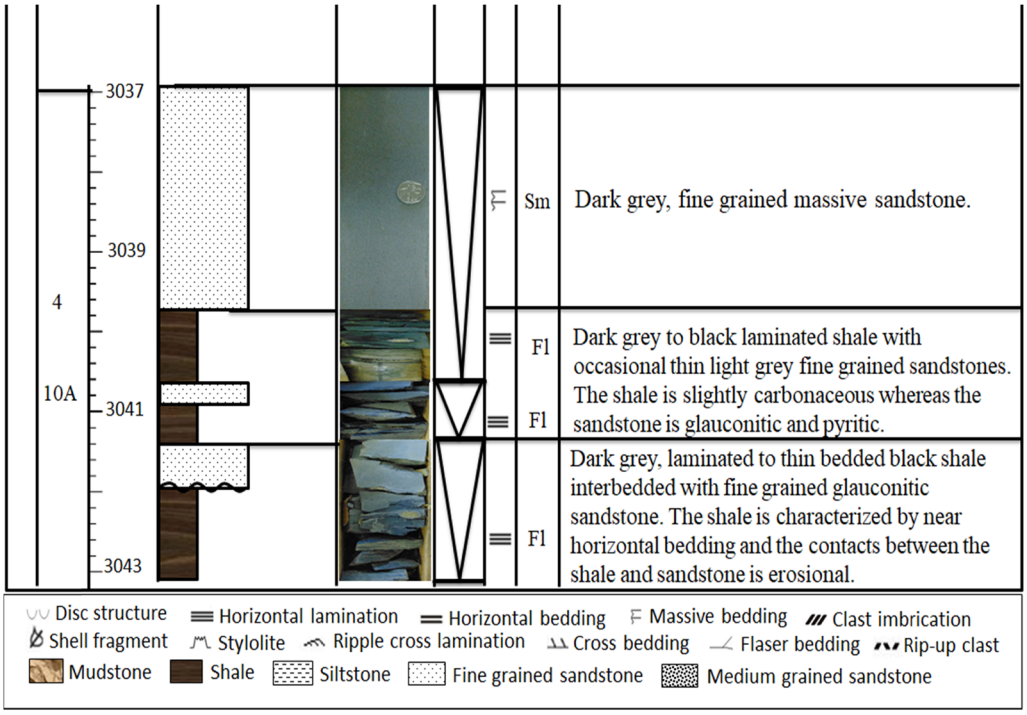
3037
3039
3041
3043
4
10A
Sm
Fl
Fl
Fl
Dark grey, fine grained massive sandstone.
Dark grey to black laminated shale with occasional thin light grey fine grained sandstones. The shale is slightly carbonaceous whereas the sandstone is glauconitic and pyritic.
Dark grey, laminated to thin bedded black shale interbedded with fine grained glauconitic sandstone. The shale is characterized by near horizontal bedding and the contacts between the shale and sandstone is erosional.
Disc structure
Horizontal lamination
Horizontal bedding
Massive bedding
Clast imbrication
Shell fragment
Stylolite
Ripple cross lamination
Cross bedding
Flaser bedding
Rip-up clast
Mudstone
Shale
Siltstone
Fine grained sandstone
Medium grained sandstone

(*Continued*)

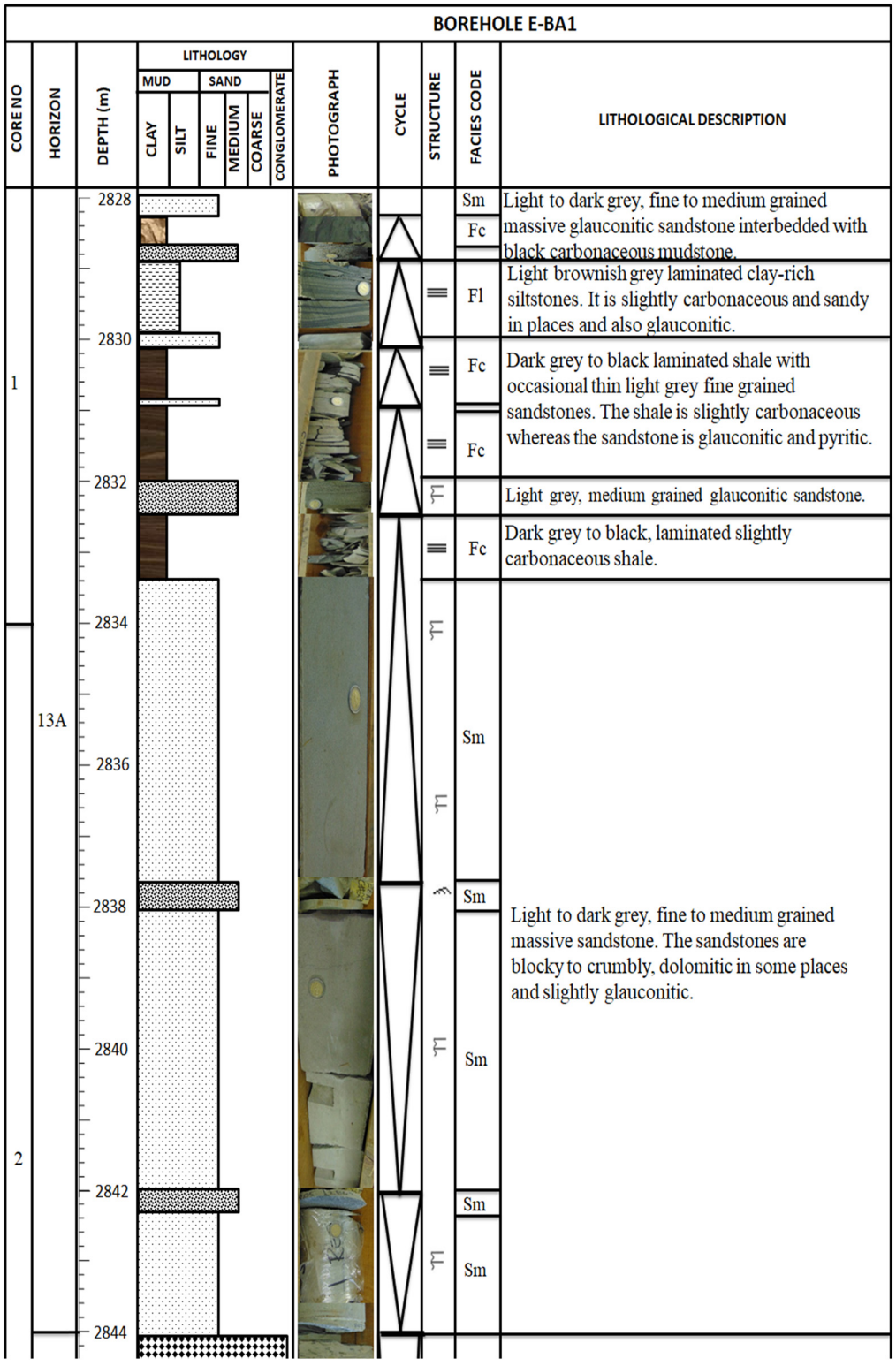
BOREHOLE E-BA1
CORE NO
HORIZON
DEPTH (m)
LITHOLOGY
MUD
SAND
CLAY
SILT
FINE
MEDIUM
COARSE
CONGLOMERATE
PHOTOGRAPH
CYCLE
STRUCTURE
FACIES CODE
LITHOLOGICAL DESCRIPTION
2828
2830
2832
2834
2836
2838
2840
2842
2844
1
2
13A
Sm
Fc
Light to dark grey, fine to medium grained massive glauconitic sandstone interbedded with black carbonaceous mudstone.
Fl
Light brownish grey laminated clay-rich siltstones. It is slightly carbonaceous and sandy in places and also glauconitic.
Fc
Fc
Dark grey to black laminated shale with occasional thin light grey fine grained sandstones. The shale is slightly carbonaceous whereas the sandstone is glauconitic and pyritic.
Light grey, medium grained glauconitic sandstone.
Fc
Dark grey to black, laminated slightly carbonaceous shale.
Sm
Sm
Sm
Sm
Sm
Light to dark grey, fine to medium grained massive sandstone. The sandstones are blocky to crumbly, dolomitic in some places and slightly glauconitic.

(*Continued*)

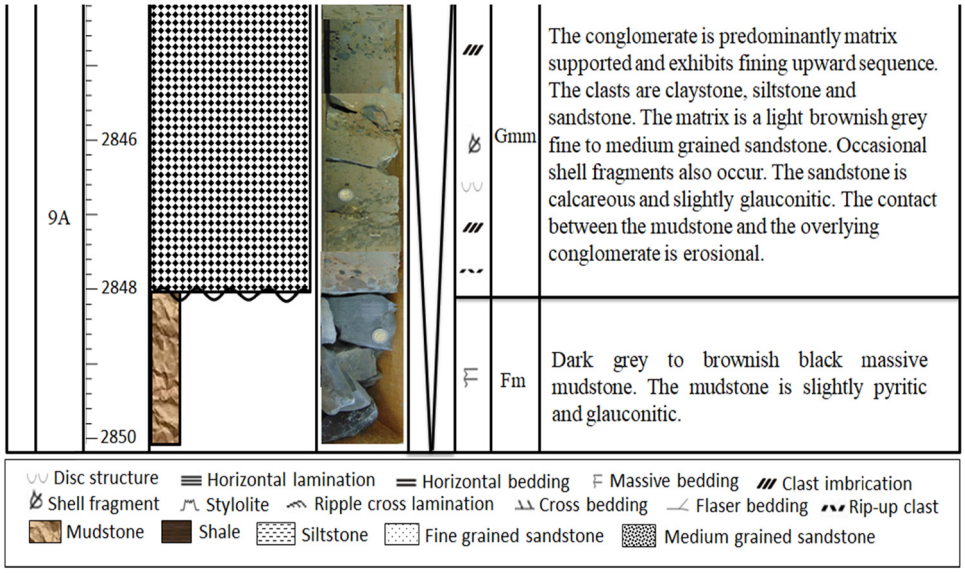
9A
2846
2848
2850
Gmm
Fm
The conglomerate is predominantly matrix supported and exhibits fining upward sequence. The clasts are claystone, siltstone and sandstone. The matrix is a light brownish grey fine to medium grained sandstone. Occasional shell fragments also occur. The sandstone is calcareous and slightly glauconitic. The contact between the mudstone and the overlying conglomerate is erosional.
Dark grey to brownish black massive mudstone. The mudstone is slightly pyritic and glauconitic.
Disc structure
Horizontal lamination
Horizontal bedding
Massive bedding
Clast imbrication
Shell fragment
Stylolite
Ripple cross lamination
Cross bedding
Flaser bedding
Rip-up clast
Mudstone
Shale
Siltstone
Fine grained sandstone
Medium grained sandstone

(*Continued*)

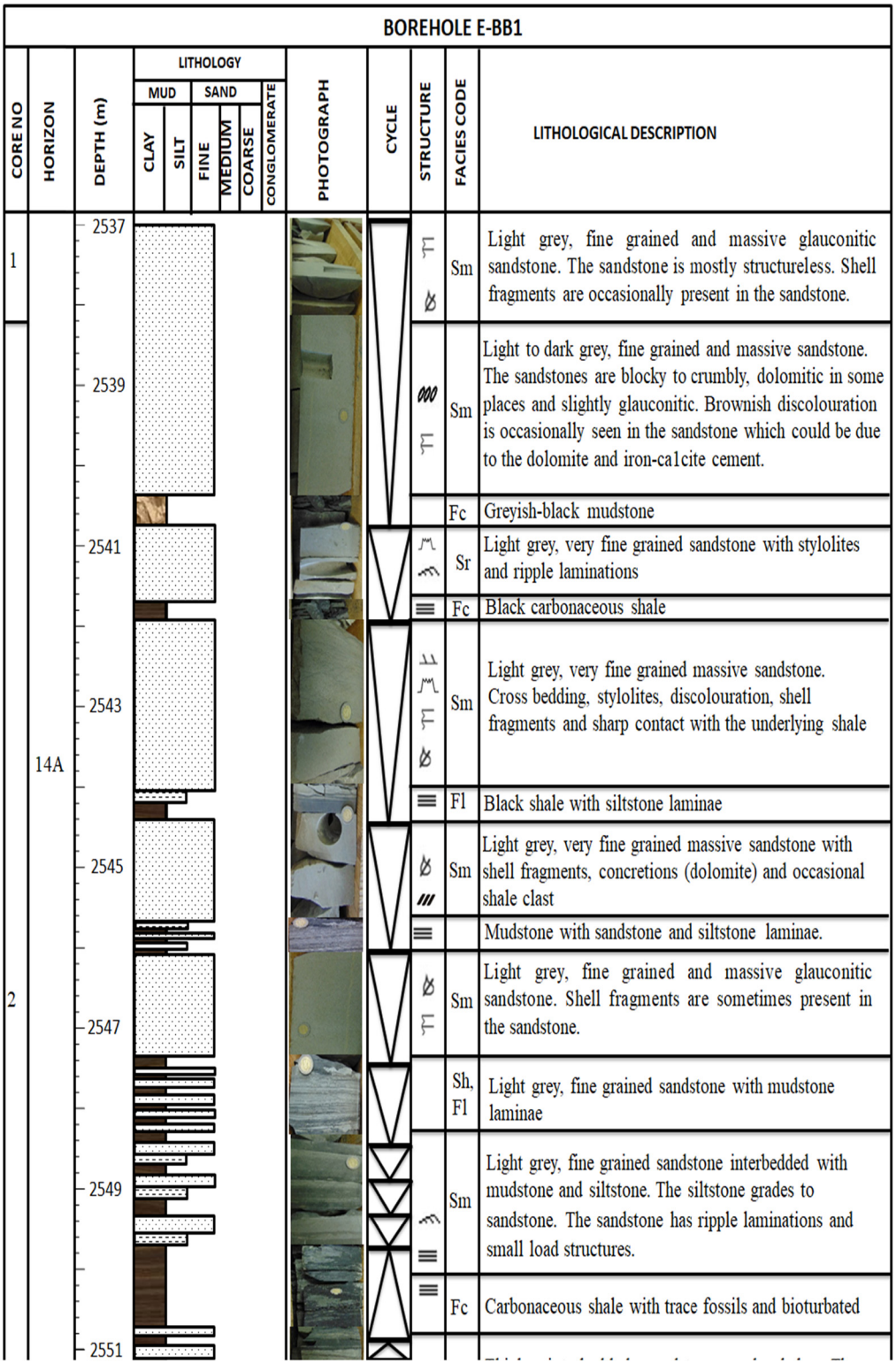
BOREHOLE E-BB1
CORE NO
HORIZON
DEPTH (m)
LITHOLOGY
MUD
SAND
CLAY
SILT
FINE
MEDIUM
COARSE
CONGLOMERATE
PHOTOGRAPH
CYCLE
STRUCTURE
FACIES CODE
LITHOLOGICAL DESCRIPTION
1
2
14A
2537
2539
2541
2543
2545
2547
2549
2551
Sm
Light grey, fine grained and massive glauconitic sandstone. The sandstone is mostly structureless. Shell fragments are occasionally present in the sandstone.
Sm
Light to dark grey, fine grained and massive sandstone. The sandstones are blocky to crumbly, dolomitic in some places and slightly glauconitic. Brownish discolouration is occasionally seen in the sandstone which could be due to the dolomite and iron-calcite cement.
Fc
Greyish-black mudstone
Sr
Light grey, very fine grained sandstone with stylolites and ripple laminations
Fc
Black carbonaceous shale
Sm
Light grey, very fine grained massive sandstone. Cross bedding, stylolites, discolouration, shell fragments and sharp contact with the underlying shale
Fl
Black shale with siltstone laminae
Sm
Light grey, very fine grained massive sandstone with shell fragments, concretions (dolomite) and occasional shale clast
Mudstone with sandstone and siltstone laminae.
Sm
Light grey, fine grained and massive glauconitic sandstone. Shell fragments are sometimes present in the sandstone.
Sh, Fl
Light grey, fine grained sandstone with mudstone laminae
Sm
Light grey, fine grained sandstone interbedded with mudstone and siltstone. The siltstone grades to sandstone. The sandstone has ripple laminations and small load structures.
Fc
Carbonaceous shale with trace fossils and bioturbated

(*Continued*)

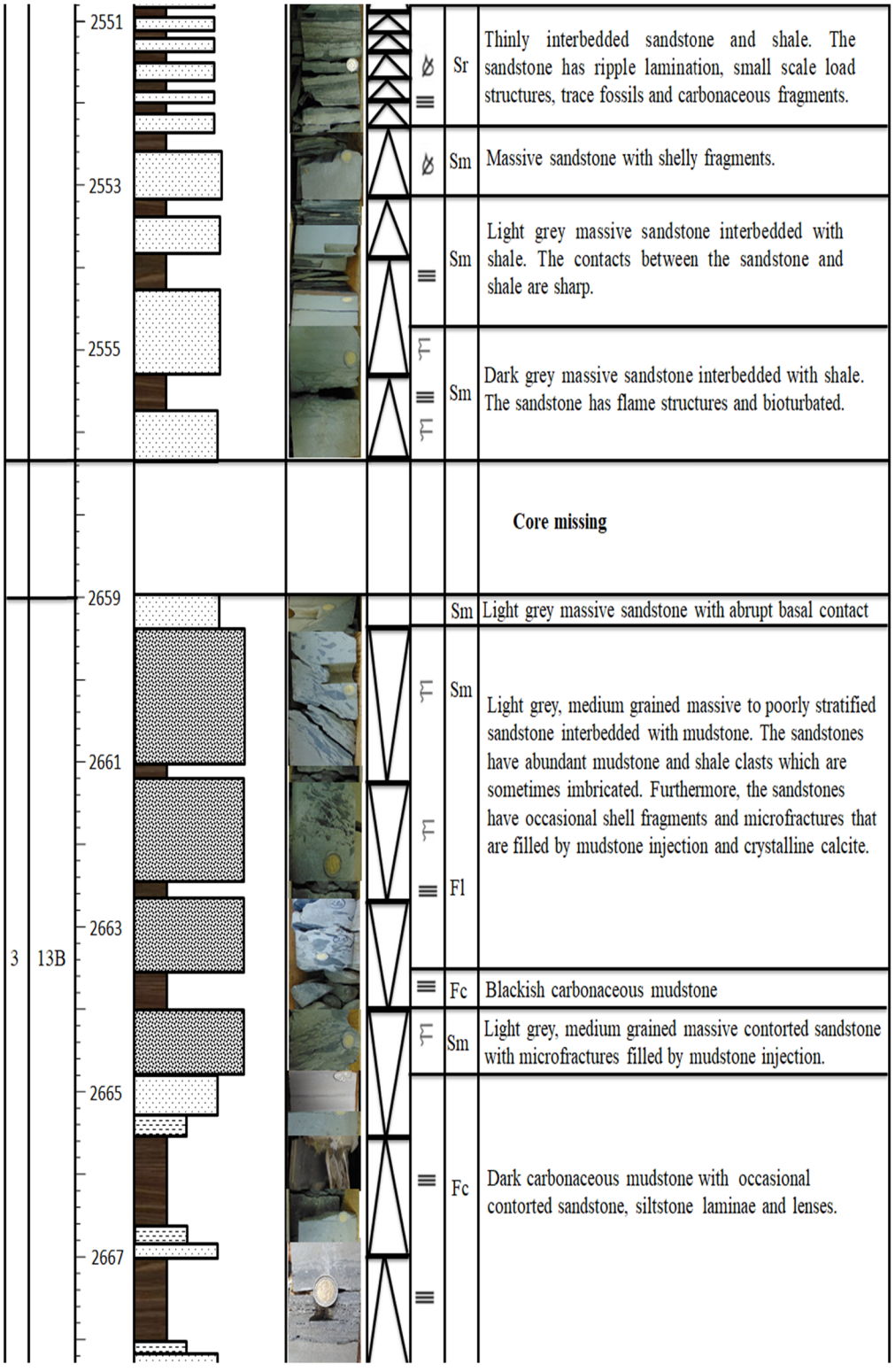
2551
2553
2555
2659
2661
2663
2665
2667
3
13B
Sr
Thinly interbedded sandstone and shale. The sandstone has ripple lamination, small scale load structures, trace fossils and carbonaceous fragments.
Sm
Massive sandstone with shelly fragments.
Sm
Light grey massive sandstone interbedded with shale. The contacts between the sandstone and shale are sharp.
Sm
Dark grey massive sandstone interbedded with shale. The sandstone has flame structures and bioturbated.
Core missing
Sm
Light grey massive sandstone with abrupt basal contact
Sm
Fl
Light grey, medium grained massive to poorly stratified sandstone interbedded with mudstone. The sandstones have abundant mudstone and shale clasts which are sometimes imbricated. Furthermore, the sandstones have occasional shell fragments and microfractures that are filled by mudstone injection and crystalline calcite.
Fc
Blackish carbonaceous mudstone
Sm
Light grey, medium grained massive contorted sandstone with microfractures filled by mudstone injection.
Fc
Dark carbonaceous mudstone with occasional contorted sandstone, siltstone laminae and lenses.

(*Continued*)

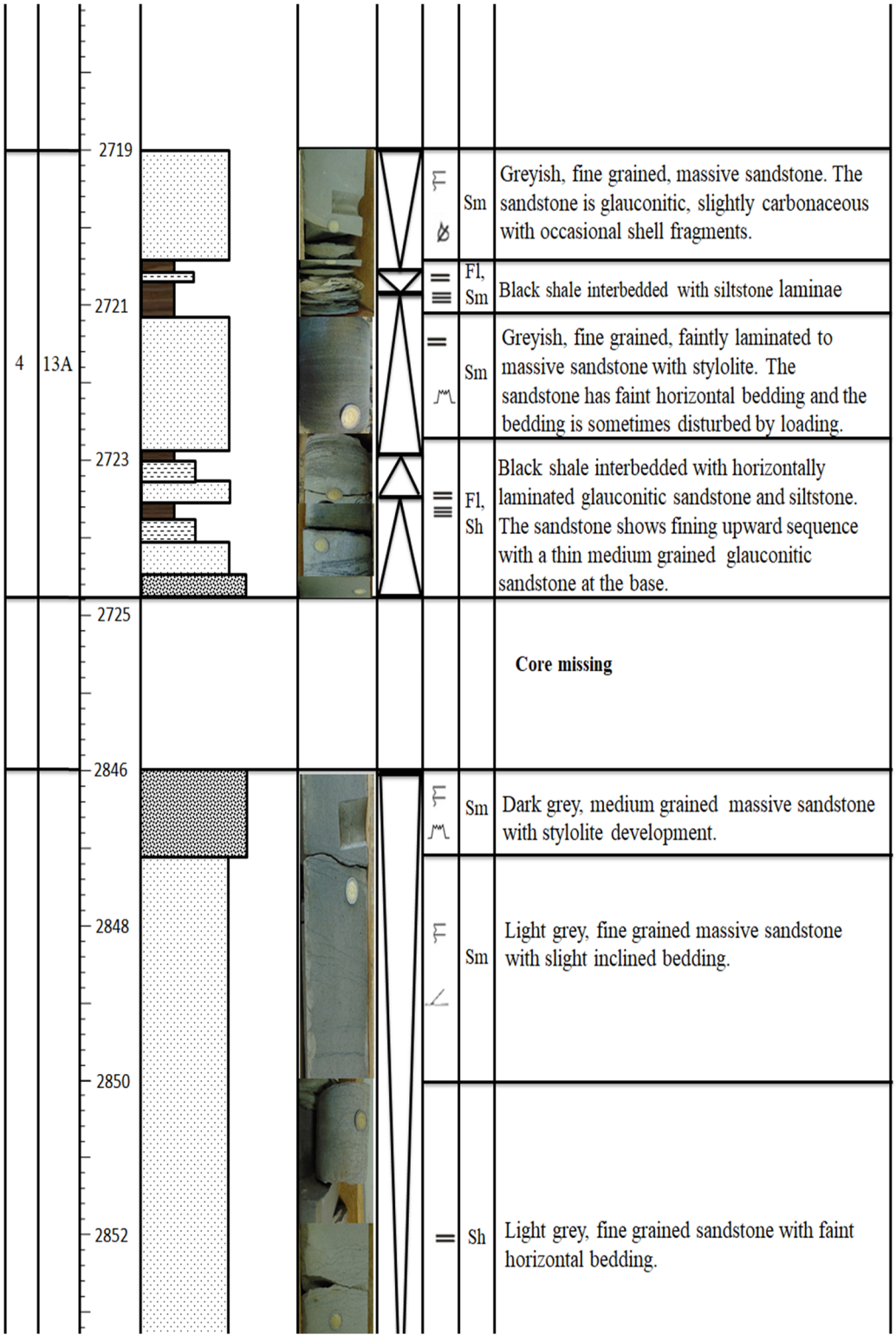
4
13A
2719
2721
2723
2725
2846
2848
2850
2852
Sm
Greyish, fine grained, massive sandstone. The sandstone is glauconitic, slightly carbonaceous with occasional shell fragments.
Fl, Sm
Black shale interbedded with siltstone laminae
Sm
Greyish, fine grained, faintly laminated to massive sandstone with stylolite. The sandstone has faint horizontal bedding and the bedding is sometimes disturbed by loading.
Fl, Sh
Black shale interbedded with horizontally laminated glauconitic sandstone and siltstone. The sandstone shows fining upward sequence with a thin medium grained glauconitic sandstone at the base.
Core missing
Sm
Dark grey, medium grained massive sandstone with stylolite development.
Sm
Light grey, fine grained massive sandstone with slight inclined bedding.
Sh
Light grey, fine grained sandstone with faint horizontal bedding.

(*Continued*)

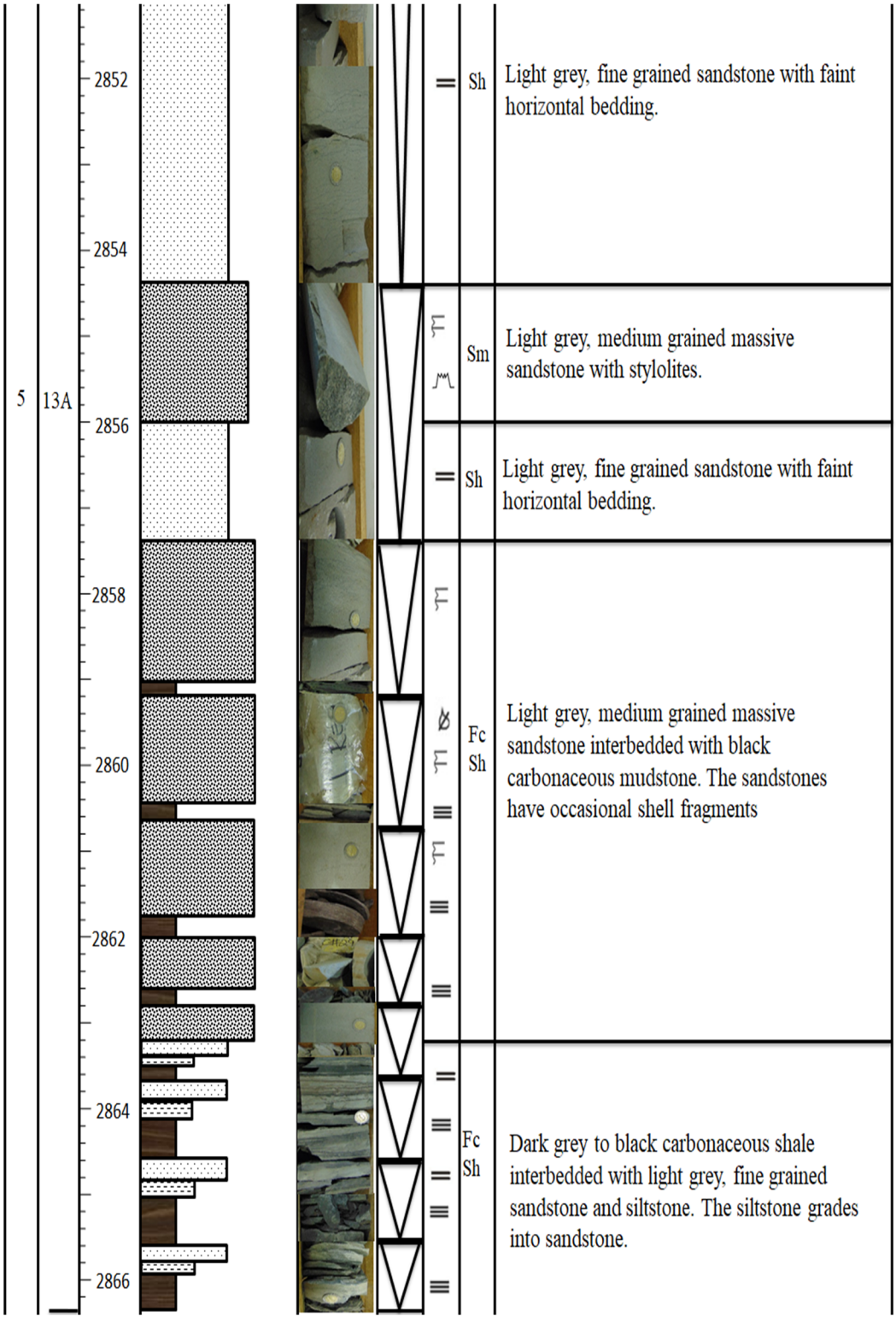
5
13A
2852
2854
2856
2858
2860
2862
2864
2866
Sh
Light grey, fine grained sandstone with faint horizontal bedding.
Sm
Light grey, medium grained massive sandstone with stylolites.
Sh
Light grey, fine grained sandstone with faint horizontal bedding.
Fc
Sh
Light grey, medium grained massive sandstone interbedded with black carbonaceous mudstone. The sandstones have occasional shell fragments
Fc
Sh
Dark grey to black carbonaceous shale interbedded with light grey, fine grained sandstone and siltstone. The siltstone grades into sandstone.

(*Continued*)

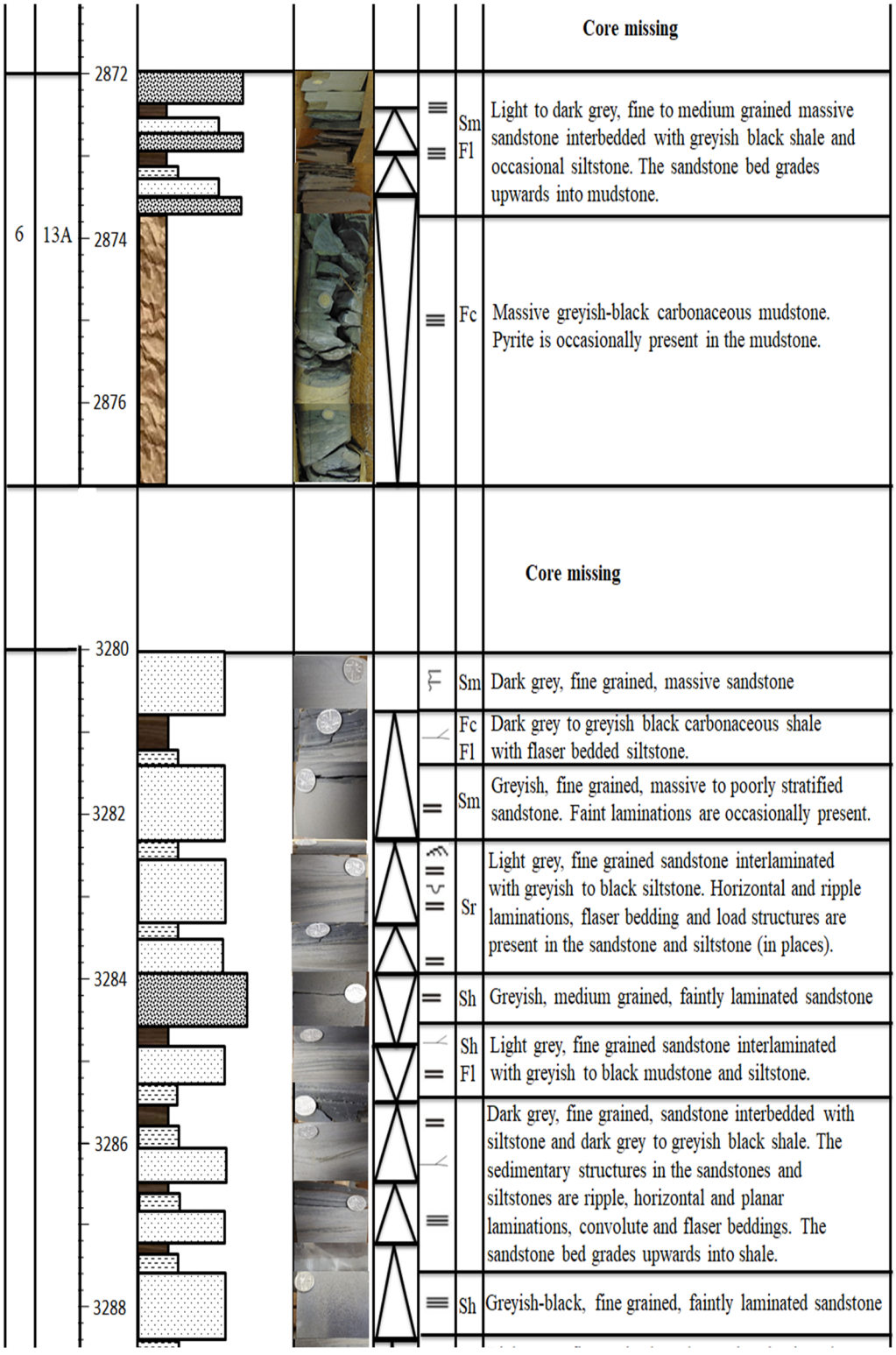
Core missing
2872
Sm
Fl
Light to dark grey, fine to medium grained massive sandstone interbedded with greyish black shale and occasional siltstone. The sandstone bed grades upwards into mudstone.
6
13A
2874
Fc
Massive greyish-black carbonaceous mudstone. Pyrite is occasionally present in the mudstone.
2876
Core missing
3280
Sm
Dark grey, fine grained, massive sandstone
Fc
Fl
Dark grey to greyish black carbonaceous shale with flaser bedded siltstone.
3282
Sm
Greyish, fine grained, massive to poorly stratified sandstone. Faint laminations are occasionally present.
Sr
Light grey, fine grained sandstone interlaminated with greyish to black siltstone. Horizontal and ripple laminations, flaser bedding and load structures are present in the sandstone and siltstone (in places).
3284
Sh
Greyish, medium grained, faintly laminated sandstone
Sh
Fl
Light grey, fine grained sandstone interlaminated with greyish to black mudstone and siltstone.
3286
Dark grey, fine grained, sandstone interbedded with siltstone and dark grey to greyish black shale. The sedimentary structures in the sandstones and siltstones are ripple, horizontal and planar laminations, convolute and flaser beddings. The sandstone bed grades upwards into shale.
3288
Sh
Greyish-black, fine grained, faintly laminated sandstone

(*Continued*)

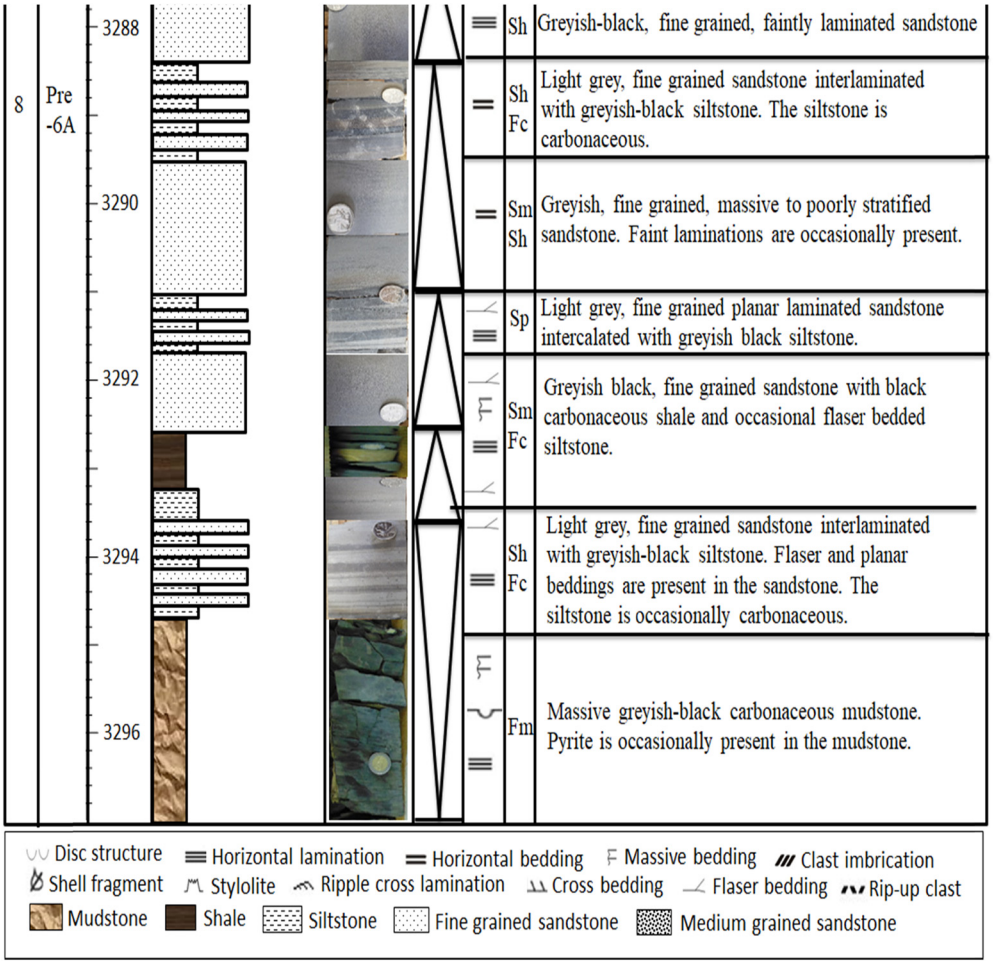
8
Pre
-6A
3288
3290
3292
3294
3296
Sh
Greyish-black, fine grained, faintly laminated sandstone
Sh
Fc
Light grey, fine grained sandstone interlaminated with greyish-black siltstone. The siltstone is carbonaceous.
Sm
Sh
Greyish, fine grained, massive to poorly stratified sandstone. Faint laminations are occasionally present.
Sp
Light grey, fine grained planar laminated sandstone intercalated with greyish black siltstone.
Sm
Fc
Greyish black, fine grained sandstone with black carbonaceous shale and occasional flaser bedded siltstone.
Sh
Fc
Light grey, fine grained sandstone interlaminated with greyish-black siltstone. Flaser and planar beddings are present in the sandstone. The siltstone is occasionally carbonaceous.
Fm
Massive greyish-black carbonaceous mudstone. Pyrite is occasionally present in the mudstone.
Disc structure
Horizontal lamination
Horizontal bedding
Massive bedding
Clast imbrication
Shell fragment
Stylolite
Ripple cross lamination
Cross bedding
Flaser bedding
Rip-up clast
Mudstone
Shale
Siltstone
Fine grained sandstone
Medium grained sandstone

(*Continued*)

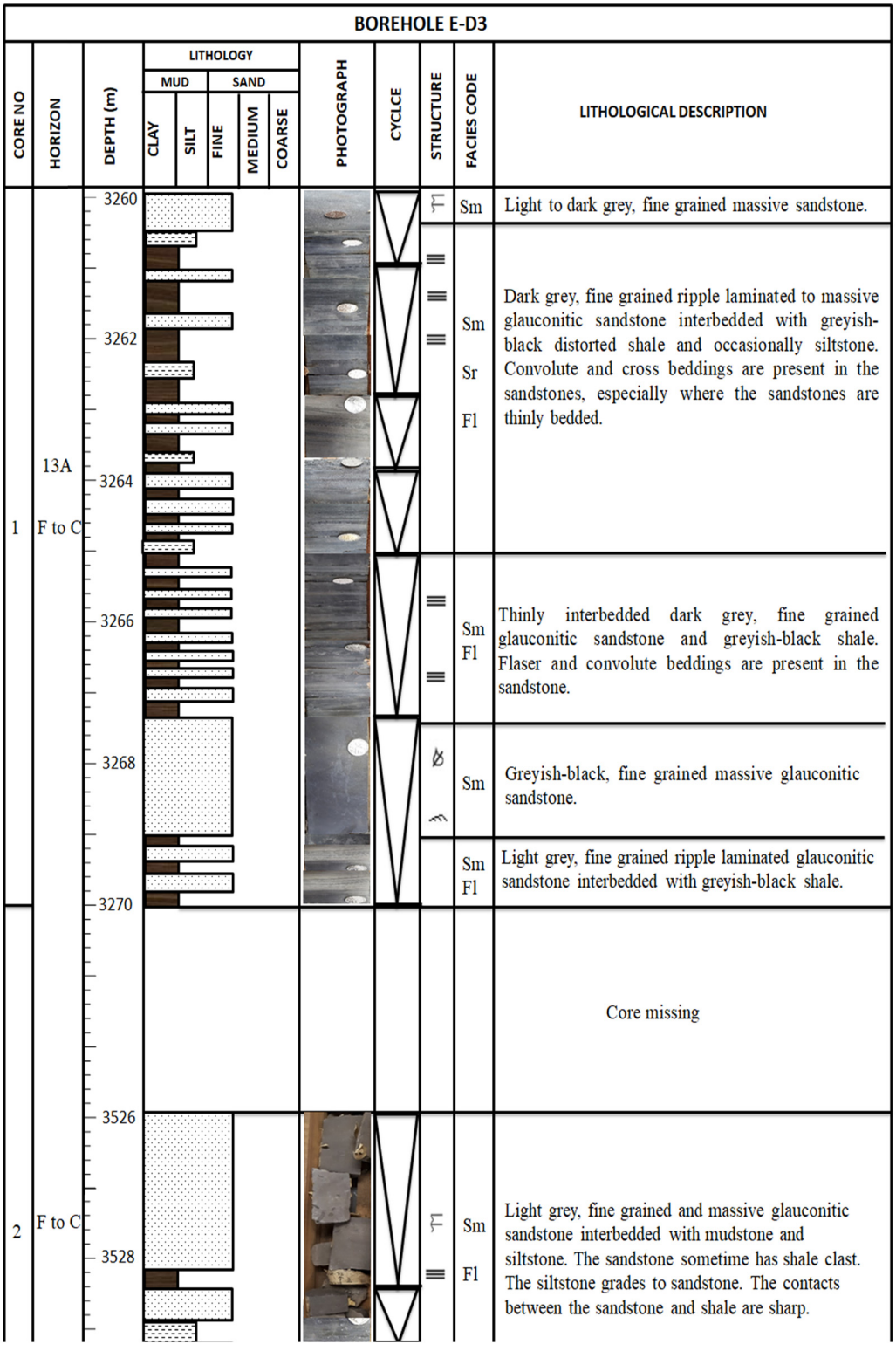
BOREHOLE E-D3
CORE NO
HORIZON
DEPTH (m)
LITHOLOGY
MUD
SAND
CLAY
SILT
FINE
MEDIUM
COARSE
PHOTOGRAPH
CYCLCE
STRUCTURE
FACIES CODE
LITHOLOGICAL DESCRIPTION
3260
3262
3264
3266
3268
3270
3526
3528
13A
F to C
1
2
F to C
Sm
Light to dark grey, fine grained massive sandstone.
Sm
Sr
Fl
Dark grey, fine grained ripple laminated to massive glauconitic sandstone interbedded with greyish-black distorted shale and occasionally siltstone. Convolute and cross beddings are present in the sandstones, especially where the sandstones are thinly bedded.
Sm
Fl
Thinly interbedded dark grey, fine grained glauconitic sandstone and greyish-black shale. Flaser and convolute beddings are present in the sandstone.
Sm
Greyish-black, fine grained massive glauconitic sandstone.
Sm
Fl
Light grey, fine grained ripple laminated glauconitic sandstone interbedded with greyish-black shale.
Core missing
Sm
Fl
Light grey, fine grained and massive glauconitic sandstone interbedded with mudstone and siltstone. The sandstone sometime has shale clast. The siltstone grades to sandstone. The contacts between the sandstone and shale are sharp.

(*Continued*)

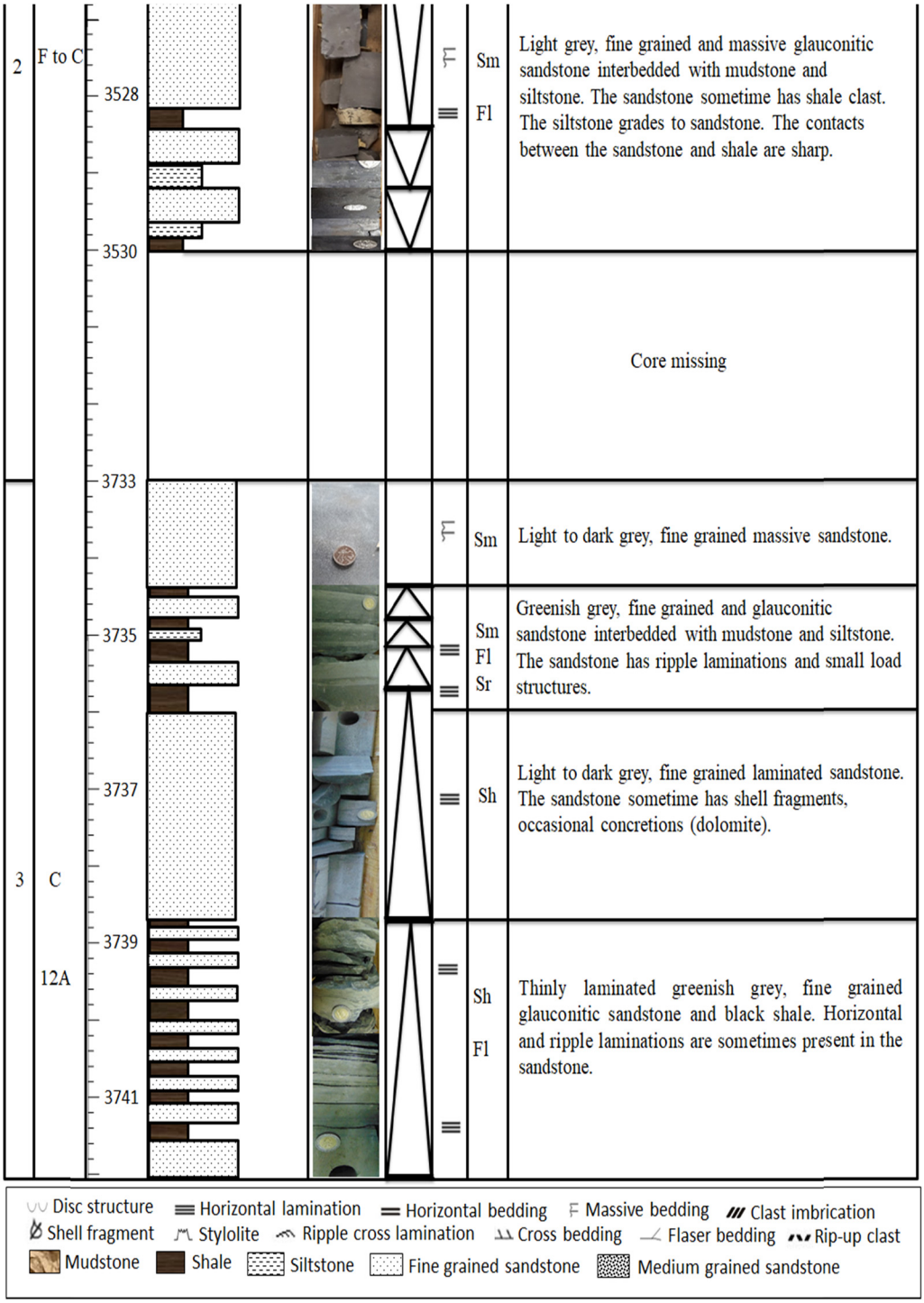

Figure A1: Stratigraphy of the Bredasdorp Basin in boreholes E-AH1, E-AJ1, E-BA1, E-BB1 and E-D3.